Accepted Manuscript

First-in-class DAPK1/CSF1R dual inhibitors: Discovery of 3,5-dimethoxy-*N*-(4-(4-methoxyphenoxy)-2-((6-morpholinopyridin-3-yl)amino)pyrimidin-5-yl)benzamide as a potential anti-tauopathies agent

Ahmed Karam Farag, Ahmed H.E. Hassan, Hyeanjeong Jeong, Youngji Kwon, Jin Gyu Choi, Myung Sook Oh, Ki Duk Park, Yun Kyung Kim, Eun Joo Roh

PII: S0223-5234(18)30926-7

DOI: https://doi.org/10.1016/j.ejmech.2018.10.057

Reference: EJMECH 10843

To appear in: *European Journal of Medicinal Chemistry*

Received Date: 1 August 2018

Revised Date: 15 October 2018

Accepted Date: 23 October 2018

Please cite this article as: A.K. Farag, A.H.E. Hassan, H. Jeong, Y. Kwon, J.G. Choi, M.S. Oh, K.D. Park, Y.K. Kim, E.J. Roh, First-in-class DAPK1/CSF1R dual inhibitors: Discovery of 3,5-dimethoxy-*N*-(4-(4-methoxyphenoxy)-2-((6-morpholinopyridin-3-yl)amino)pyrimidin-5-yl)benzamide as a potential anti-tauopathies agent, *European Journal of Medicinal Chemistry* (2018), doi: https://doi.org/10.1016/j.ejmech.2018.10.057.

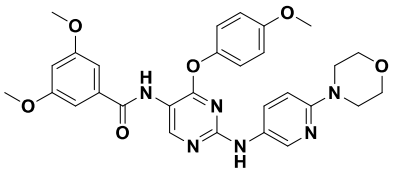

Compound 3l

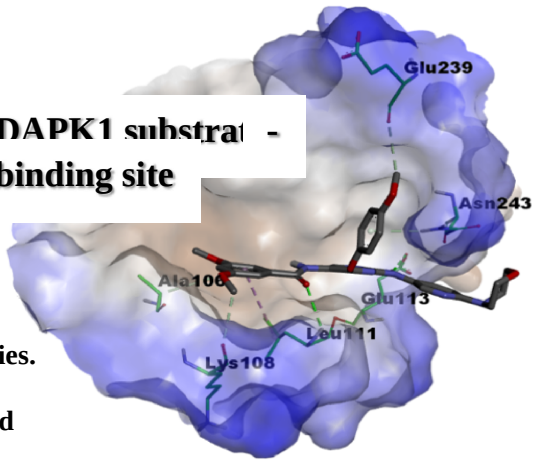

- **CSF1R IC_{50} = 0.15 µM.**
- **DAPK1 IC_{50} = 1.25 µM.**
- **Non-ATP-competitive inhibition of DAPK1.**
- **No inhibition of any of the DAPK or PDGFR families.**
- **Inhibition of tau aggregation IC_{50} = 5.0 µM.**
- **55% inhibition in NO production in LPS-stimulated BV-2 microglial cells.**
- **No inhibition for hERG.**
- **PAMPA-BBB = high permeability.**

First-in-Class DAPK1/CSF1R Dual Inhibitors: Discovery of 3,5-Dimethoxy-*N*-(4-(4-methoxyphenoxy)-2-((6-morpholinopyridin-3-yl)amino)pyrimidin-5-yl)benzamide as a Potential Anti-Tauopathies Agent

Ahmed Karam Farag[a,b,1], Ahmed H. E. Hassan[c,d], Hyeanjeong Jeong[e,f], Youngji Kwon[g], Jin Gyu Choi[h], Myung Sook Oh[g], Ki Duk Park[b,i], Yun Kyung Kim[b,e], Eun Joo Roh[a,b*]

[a] *Chemical Kinomics Research Center, Korea Institute of Science and Technology (KIST), Seoul 02792, Republic of Korea.*

[b] *Division of Bio-Medical Science &Technology, KIST School, University of Science and Technology, Seoul 02792, Republic of Korea.*

[c] *Department of Medicinal Chemistry, Faculty of Pharmacy, Mansoura University, Mansoura, 35516, Egypt.*

[d] *Medicinal Chemistry Laboratory, Department of Pharmacy, College of Pharmacy, Kyung Hee University, Seoul 02447, Republic of Korea.*

[e] *Brain Science Institute, Convergence Research Center for Diagnosis, Treatment and Care System of Dementia, Korea Institute of Science and Technology (KIST), Seoul, 02791, Republic of Korea.*

[f] *Department of Life Science, Korea University, Seoul, 02841, Republic of Korea.*

[g] *Department of Life and Nanopharmaceutical Sciences, Graduate School, Kyung Hee University, Seoul, Republic of Korea.*

[h] *BK21 PLUS Integrated Education and Research Center for Nature-inspired Drug Development Targeting Healthy Aging, Kyung Hee University, Seoul, Republic of Korea.*

[i] *Convergence Research Center for Diagnosis, Treatment and Care System of Dementia, Korea Institute of Science and Technology (KIST), Republic of Korea.*

[*]**Corresponding author:** Eun Joo Roh

Email address: r8636@kist.re.kr

Postal address: Korea Institute of Science and Technology, Materials and Life Science Research Division, Chemical Kinomics Research Center, Hwarang-ro 14-gil 5, Seongbuk-gu, Seoul, Republic of Korea, 02792.

[1] Current affiliation and address: RI Translational Research Team, Division of Applied RI, Korea Institute of Radiological and Medical Sciences (KIRAMS), 75 Nowon-ro, Nowon-gu, Seoul, Republic of Korea, 01812

Abstract

Kinase irregularity has been correlated with several complex neurodegenerative tauopathies. Development of selective inhibitors of these kinases might afford promising anti-tauopathy therapies. While DAPK1 inhibitors halt the formation of tau aggregates and counteract neuronal death, CSF1R inhibitors could alleviate the tauopathies-associated neuroinflammation. Herein, we report the design, synthesis, biological evaluation, mechanistic study, and molecular docking study of novel CSF1R/DAPK1 dual inhibitors as multifunctional molecules inhibiting the formation of tau aggregates and neuroinflammation. Compound **3l**, the most potent DAPK1 inhibitor in the *in vitro* kinase assay (IC_{50} = 1.25 μM) was the most effective tau aggregates formation inhibitor in the cellular assay (IC_{50} = 5.0 μM). Also, compound **3l** elicited potent inhibition of CSF1R in the *in vitro* kinase assay (IC_{50} = 0.15 μM) and promising inhibition of nitric oxide production in LPS-induced BV-2 cells (55% inhibition at 10 μM concentration). Kinase profiling and hERG binding assay anticipated the absence of off-target toxicities while the PAMPA-BBB assay predicted potentially high BBB permeability. The mechanistic study and selectivity profile suggest compound **3l** as a non-ATP-competitive DAPK1 inhibitor and an ATP-competitive CSF1R inhibitor while the *in silico* calculations illustrated binding of compound **3l** to the substrate-binding site of DAPK1. Hence, compound **3l** might act as a protein-protein interaction inhibitor by hindering DAPK1 kinase reaction through preventing the binding of DAPK1 substrates.

Keywords

DAPK1; CSF1R; Tauopathies; Neuroinflammation; multifunctional molecules.

1. Introduction

The decline of mental capacities caused by chronic neurodegenerative disorders is the largest global source of disabilities producing more than 20% of the "Years Lived with Disability (YLD)" which is a measurement for a disease burden [1]. Among neurodegenerative diseases, tauopathies emerge as a large class of more than twenty-five diseases characterized by neurodegeneration accompanied by the formation of filamentous aggregates of hyperphosphorylated microtubule-associated protein (MAP) tau within the CNS [2, 3]. Alzheimer's disease (AD) is the most common tauopathy, while relatively less encountered tauopathies include post-encephalitic parkinsonism, Pick's disease, progressive supranuclear palsy (PSP) and corticobasal degeneration (CBD) [4, 5]. The currently available therapies provide only symptomatic treatments without halting or slowing down the progression of these diseases. Certainly, there is an urgent need to develop an effective treatment for this class of diseases that address their underlying causes.

Despite the high solubility of tau proteins, anomalously hyperphosphorylated tau protein aggregates into neurofibrillary tangles (NFTs), the hallmark of tauopathies [6]. It is known that this hyperphosphorylation converts the normally functioning tau protein into a neurotoxin that triggers neuronal death. Accordingly, research to identify small molecule inhibitors of tau hyperphosphorylation is a promising strategy towards the development of an effective therapy [6, 7]. Death-associated protein kinase 1 (DAPK1) was recently discovered as a valid therapeutic target for neurodegenerative diseases [8-10]. The role of DAPK1 as a novel regulator of tau phosphorylation indicates that its upregulation might be involved in tauopathies. Recent reports illustrated that DAPK1 regulates tau protein by direct phosphorylation of Thr231, Ser262, and

Ser396 and indirectly via phosphorylating tau regulatory proteins such as peptidyl-prolyl cis-trans isomerase NIMA-interacting 1 (PIN1) and microtubule affinity-regulating kinase 1/2 (MARK1/2) [8]. These actions are believed to mediate tau protein hyperphosphorylation and subsequent formation of NFTs. In addition, DAPK1, being a strong regulator of apoptosis and autophagy mediates neuronal cell death via phosphorylating N-myc downstream-regulated gene 2 (NDRG2) ultimately triggering neuronal cell death. In fact, anomalous deregulation and hyperphosphorylation of tau protein are strongly correlated with DAPK1 activation [11-13]. Therefore, inhibition of DAPK1 might be beneficial for the treatment of tauopathies. To the best of our knowledge, no clinically useful DAPK1 inhibitor has been realized yet despite the validation of DAPK1 as a viable drug target [14].

In addition to NFTs of hyperphosphorylated tau protein, reactive gliosis; a continuous glial cells activation is a hallmark that characterizes tauopathies. It establishes a chronic neuroinflammatory process resulting in the production of inflammatory mediators that eventually contribute to the progression of the disease [15-18]. In contrast to the previous belief that neuroinflammation arises as a result of neurodegeneration, recent evidence showed that the activation of microglia and neuroinflammation precede the aggregation and formation of tau tangles [19]. In a repetitive cycle, the formed aggregates trigger a more inflammatory response that produces more inflammatory mediators which contribute to the formation of more protein aggregates through various mechanisms [20].

Microglia are innate immune cells residing in the brain. They exist in a dormant state under non-pathological conditions [21]. However, the chronic activation of microglia results in a reactive gliosis which contributes to the neurodegeneration observed in several tauopathies such as AD, parkinsonism, Pick's disease and chronic traumatic encephalopathy [22-24]. Culminated

pieces of evidence showed that the inflammatory component is crucial for the initiation and development of tauopathies [25-28]. The kinase known as colony stimulating factor 1 receptor (CSF1R; also known as macrophage colony-stimulating factor receptor; M-CSFR) is a key regulator of survival and proliferation of the microglial cells [29, 30]. Several reports showed that inhibition of CSF1R results in a reduction of microglia-dependent neuroinflammation and slowing down the progression of neurodegenerative diseases [31, 32]. In addition, the use of a CSF1R inhibitor to deplete microglia was found to inhibit the transmission of tau protein from neuron to neuron and reduce the microglial-assisted neurotoxicity [33]. Collectively, these reports emphasize the significance of developing CSF1R inhibitors targeting microglia as potential therapeutics for neurodegenerative diseases.

For successful evasion of the vicious cycle of neuroinflammation-protein aggregates formation, it might be more useful to target both of the two major elements of the cycle. Towards achieving this goal, two strategies might be possible: development of a combination therapy or development of a multifunctional single molecule targeting both NFTs formation and neuroinflammation. A multifunctional single molecule is believed to be a more favorable strategy in terms of pharmacokinetic and pharmacodynamic advantages, as well as, lowering side effects and toxicity [34, 35]. Bearing these aims and concepts in our minds, we sought the development of a single small molecule inhibitor of both DAPK1 and CSF1R as first-in-class inhibitors of tau phosphorylation and neuroinflammation. Herein, we report our approach and promising results.

2. Results and Discussion

2.1. Ligands design

Recently, an imidazopyridazine inhibitor of DAPK1 (**1**; Figure 1) that binds the ATP binding site of DAPK1 was reported as a starting point for the development of DAPK1 inhibitors as potential neuroprotective agents [36]. The co-crystal structure of compound **1** with DAPK1 (PDB code: 4TXC) showed that N-1 of the imidazopyridazine moiety anchors the Val96 of the hinge region with a single hydrogen bond. The back hydrophobic pocket I of the ATP binding site is occupied by the hydroxylmethoxyphenyl moiety of compound **1** showing several polar hydrogen bonding interactions, while the hydrophobic pocket II of the ATP binding site is vacant and the aliphatic chain extends toward the solvent exposure area.

On the other hand, we have previously reported a series of potent phenoxypyrimidine scaffold-based inhibitors of CSF1R [37]. In the conducted molecular simulation study reported for our previously developed CSF1R inhibitors, compound **2** showed binding mode within the ATP binding site of CSF1R in which the 4-morpholinophenyl moiety was directed towards a hydrophobic pocket and the substituent on the phenoxy moiety showed interaction with β3 near the hinge region. Meanwhile, the 3,5-dimethoxyphenyl moiety of compound **2** was directed towards the solvent exposure region. This might indicate that manipulation of the (3,5-dimethoxybenzylidene)amino moiety at position 5 while retaining a substituted-phenoxy moiety at position 4 and a substituted phenyl moiety attached to the amino group of the core pyrimidine-2-amine might maintain the CSF1R inhibitory profile. Accordingly, modified molecules possessing the general structure **3** might act as CSF1R inhibitors (Figure 1). Based on this, we have used compound **2** as a starting point to develop small molecules dual inhibitors of DAPK1 and CSF1R.

In this regard, we anticipated that the pyrimidine-2-amine core of the modified compounds (**3**) might functionally replace the imidazopyridazine moiety of compound **1** in binding the hinge

region, while the substituted-phenyl moiety on the amino group might occupy the vacant hydrophobic pocket II of the ATP binding site of DAPK1. The imine linker of compound **2** might be replaced by an amide group to keep a proper distance between the hinge binder and the hydrophobic pocket-binding moiety. As the hydroxylmethoxyphenyl moiety of compound **1** showed several polar hydrogen bonding interactions within the hydrophobic pocket I of the ATP binding site of DAPK1, it was planned to set R^2 to either a phenyl group substituted with groups capable of forming polar interactions; or to a simple amino group. The latter was planned to explore whether only polar hydrogen bonding interactions of the introduced amino group is sufficient for activity or a hydrophobic group is also necessary. Additionally, in the proposed design, it was planned to explore the impact on activity resulting from:

(i) Variation of the R^1 substituent at the phenoxy moiety,

(ii) Replacement of the morpholino moiety with other groups,

(iii) Incorporation of nitrogen atom into the phenyl moiety attached to the amino group of the core pyrimidine-2-amine.

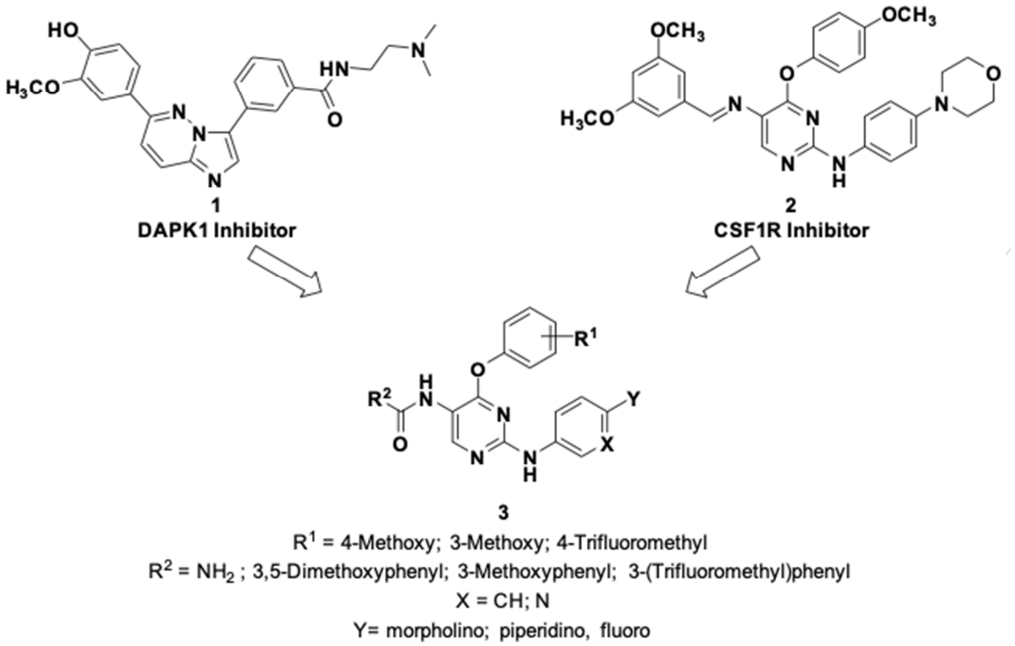

Figure 1. The proposed design of DAPK1-CSF1R dual inhibitors.

2.2. Chemistry

The targeted compounds were prepared according to Scheme 1. The required starting 2-chloro-5-nitro-4-phenoxypyrimidine derivatives **4a–c** were prepared as reported previously [37]. Nucleophilic aromatic substitution of the chlorine atom at position 2 of derivatives **4a–c** with various aromatic amines yielded 5-nitro-4-phenoxy-*N*-aryl pyrimidin-2-amine derivatives **5a–f**. Palladium-catalyzed hydrogenation of the nitro group of the derivatives **5a–f** afforded the corresponding amino derivatives **6a–f**. The urea derivatives **3a–f** were prepared by stirring an acetic acid solution of compounds **6a–f** with a concentrated aqueous solution of excess potassium cyanate at room temperature. The reaction of the amino derivatives **6a–f** with various acid chlorides at low temperature followed by warming to ambient temperature afforded the primary amides **3g–l**. Addition of the acid chlorides at low temperature was crucial for

minimizing the formation of the di-acylated products which were detected when only ice bath was used resulting in a considerable reduction of the obtained yield.

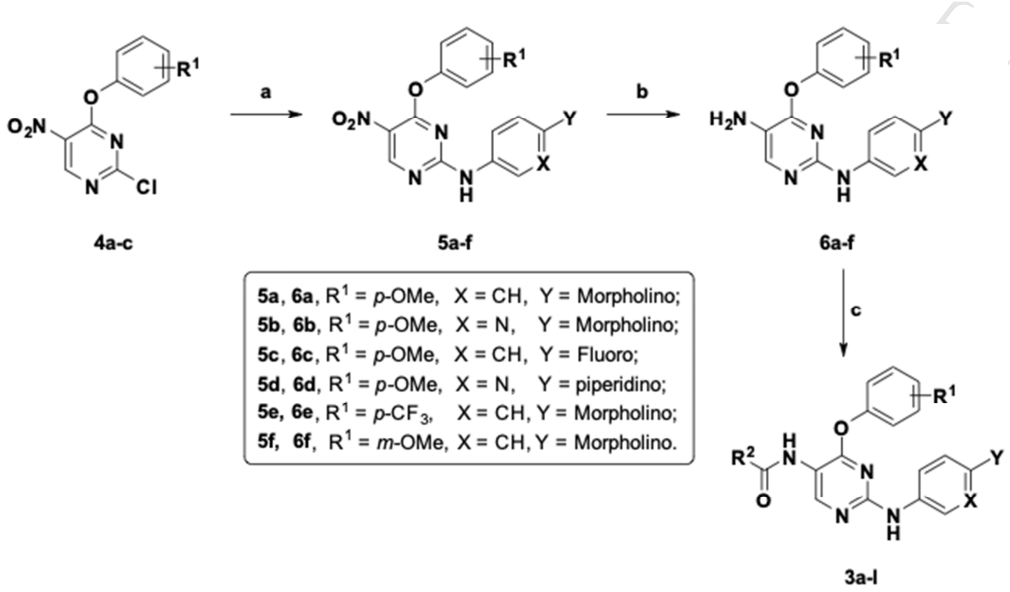

Scheme 1. Synthesis of compounds **3a–l**. Reagents and conditions: (a) appropriate amine, pyridine, THF, 80 °C, 4 h; (b) H_2, 10% Pd/C, MeOH, rt, 12 h; (c) for compounds **3a-f**: potassium cyanate, glacial acetic acid, rt, 2 h; for compounds **3g-l**: appropriate acid chloride, DIPEA, DCM, –78 °C to rt, 2 h.

The arylamine derivatives required for the preparation of compounds **5a–f** were prepared as depicted in **Scheme 2** following the reported procedures [38-40]. Thus, the activated halogens (chloro or fluoro) at the para- position to the nitro group of compounds **7a,b** were displaced with secondary amines such as morpholine or piperidine in a nucleophilic aromatic substitution reaction to provide nitro derivatives **8a–c**. Catalytic hydrogenation of the nitro derivatives afforded the required arylamine derivatives **9a–c**.

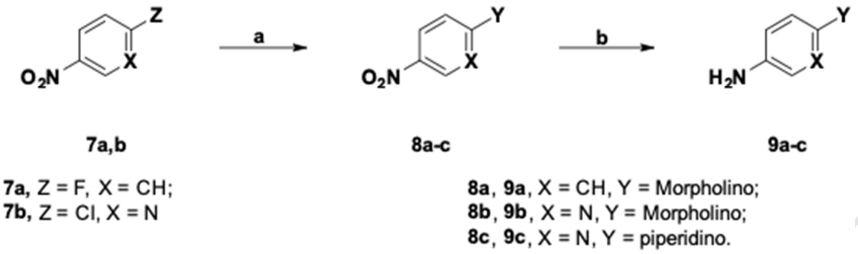

Scheme 2. Synthesis of compounds **9a–c**. Reagents and conditions: (a) appropriate amine, THF, 70 °C, 2 h (b) H_2, 10% Pt/C, MeOH, rt, 12 h.

2.3. *In vitro* kinase assay

In an initial attempt to evaluate the efficacy of the prepared compounds on the kinase reaction of CSF1R and DAPK1, the compounds were assayed in a single-dose mode (10 μM except for compounds **3a** and **3b**) in a duplicate radioisotope-based assay (Table 1). In all cases, ATP concentration of 10 μM was used and the *in vitro* kinase assay was conducted according to Reaction Biology Corporation's HotSpot^{SM} methodology. This assay method is a radiometric assay that directly measures the phosphorylated substrate that is the direct outcome of the kinase catalytic activity [41]. Compounds eliciting high percent of inhibition of the kinase reaction were subsequently evaluated for their respective IC_{50} values to measure their potencies.

Table 1. Substitution pattern, Percent inhibition values and IC_{50} values for the newly synthesized compounds over CSF1R and DAPK1.

Compd.	R^1	X	Y	R^2	CSF1R		DAPK1	
					% Inhibition ± SD values[a]	IC_{50} ± SD values (μM)[b]	% Inhibition ± SD values[a]	IC_{50} ± SD values (μM)[b]
3a	4-CH_3O	CH		NH_2	65.02 ± 0.70	4.42 ± 0.08	10.79 ± 7.10 [c]	ND [d]
3b	4-CF_3	CH		NH_2	59.61 ± 0.29	ND [d]	44.91 ± 3.10 [c]	14.30 ± 6.31

3c	3- CH_3O	CH		NH_2	**77.58 ± 0.64**	1.29 ± 0.02	15.83 ± 2.63	ND [d]
3d	4- CH_3O	CH	F	NH_2	20.99 ± 6.86	ND [d]	17.11 ± 0.08	ND [d]
3e	4- CH_3O	N		NH_2	35.43 ± 0.56	ND [d]	19.71 ± 2.04	ND [d]
3f	4- CH_3O	N		NH_2	28.44 ± 2.99	ND [d]	31.71 ± 4.25	ND [d]
3g	4- CH_3O	CH		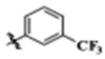	**74.70 ± 1.28**	4.89 ± 0.18	**69.70 ± 1.19** [c]	**2.61 ± 0.31**
3h	4- CH_3O	CH		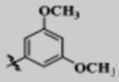	**95.34 ± 1.28**	**0.12 ± 0.003**	**65.95 ± 2.21** [c]	**2.77 ± 0.41**
3i	4- CH_3O	CH		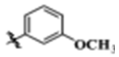	**91.85 ± 1.31**	0.78 ± 0.04	**75.06 ± 1.26**	7.44 ± 2.81
3j	4- CH_3O	N		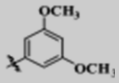	**75.99 ± 0.49**	1.72 ± 0.04	**67.28 ± 2.95**	**2.69 ± 0.21**
3k	4- CH_3O	CH	F	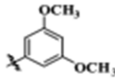	35.20 ± 6.99	ND [d]	**65.00 ± 0.70**	4.29 ± 0.23
3l	4- CH_3O	N		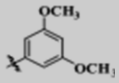	**77.94 ± 0.52**	**0.15 ± 0.006**	**66.22 ± 0.26**	**1.25 ± 0.35**

[a] The mean % inhibition of 10 μM concentration of two independent experiments.
[b] The mean values of IC_{50} calculated from duplicate 10-dose IC_{50} assay with 3-fold serial dilution starting at 20 μM.
[c] The mean % inhibition of 20 μM concentration of two independent experiments.
[d] ND, not determined.

First, the urea compounds **3a–c** in which R^2 was set to amino group and the arylamine moiety was set to 4-morpholinoaniline were prepared and evaluated. As shown in Table 1, the 10 μM dose of these compounds were capable of inhibiting the kinase reaction of CSF1R by around 60% or more. Among these compounds, the best inhibition of CSF1R kinase reaction was elicited when the substitution on the phenoxy moiety was set to 3-methoxy (compound **3c**; inhibition=77.58%), while the 4-trifluoromethyl substitution resulted in the least effective CSF1R inhibitor (compound **3b**; inhibition=59.61%). The 10 μM concentration of compound **3a** which possesses a 4-methoxy substituent on the phenoxy moiety elicited average inhibition of

CSF1R (inhibition=65.02%). However, it elicited micromolar IC_{50} value for CSF1R inhibition. Compound **3c** showed higher IC_{50} value (1.29 μM) which is consistent with its higher inhibition percent. When these three compounds were tested for inhibition of DAPK1 kinase reaction, compound **3c** that elicited the highest potency against CSF1R showed a very low inhibition percent against DAPK1. Accordingly, compounds **3a** and **3b** were tested for DAPK1 inhibition at a concentration of 10 μM. Nevertheless, both compounds **3a** and **3b** elicited low inhibition of DAPK1 with a measured IC_{50} value of 14.30 μM for compound **3b**, which elicited the highest DAPK1 inhibition among these three compounds. Because compound **3b**, which possesses a 3-trifluoromethyl substituent on the phenoxy moiety was the least effective CSF1R inhibitor among these compounds, while compounds bearing methoxy substituents were more effective CSF1R inhibitors, all further synthesized compounds possessed 4-methoxy substituent on the phenoxy moiety. Thus, compounds **3d–f** were prepared via modification of the 4-morpholinoaniline moiety. *In vitro* kinase assay showed that replacement of the morpholine moiety by fluorine atom afforded compound with reduced efficiency for inhibition of CSF1R, yet did not significantly enhance the measured inhibition percent of DAPK1 (compound **3d**; Table 1). Similarly, replacement of the aniline moiety by the heterocyclic aminopyridine alone (compound **3e**; Table 1) or when combined with changing the morpholine moiety into piperidine (compound **3f**; Table 1) did not result in compounds eliciting any promising inhibition percent against both of DAPK1 and CSF1R.

Next, amide compounds in which R^2 was set to a substituted-phenyl moiety were prepared and evaluated. Because we found that the 4-morpholinoaniline, the 4-methoxyphenyl as arylamine, and the phenoxy moieties relatively afforded compounds with viable inhibitory activity against CSF1R, these moieties were retained in the prepared amide compounds **3g–l**,

while R^2 was varied. The results of the *in vitro* kinase assay showed that all of these amide compounds retained the inhibitory activity against CSF1R but gained a promising inhibitory activity against DAPK1. While the 3,5-dimethoxyphenyl moiety bestowed compound **3g** with excellent inhibitory activity against CSF1R (IC_{50}= 0.12 μM; Table 1) and good inhibitory activity against DAPK1 (IC_{50}= 2.77 μM; Table 1), the 3-dimethoxyphenyl moiety rendered compound **3i** less potent DAPK1 inhibitor (IC_{50}= 7.44 μM; Table 1) and also slightly diminished its inhibitory activity against CSF1R (IC_{50}= 0.78 μM; Table 1). On the other hand, the 3-trifluoromethylphenyl moiety in compound **3g** resulted in severe deterioration of the inhibitory activity against CSF1R (IC_{50}= 4.89 μM; Table 1) despite retaining good inhibitory activity against DAPK1 (IC_{50}= 2.61 μM; Table 1). Therefore, another three compounds **3j–l** were prepared so that the R^2 group is fixed to 3,5-dimethoxyphenyl moiety while the variations in the arylamine moiety were explored. The results showed that 4-fluoroaniline as the arylamine moiety in compound **3k** almost doubled the IC_{50} value of DAPK1 and resulted in the loss of potential inhibitory activity against CSF1R. Relative to compound **3h**, compound **3l** in which the 4-morpholinoaniline was changed to 4-morpholino-pyridinamine showed improvement of the IC_{50} value against DAPK1 while the potency against CSF1R was retained (Table 1). However, when the isosteric 4-piperidino-pyridinamine was used for compound **3j** in place of the 4-morpholino-pyridinamine moiety of compound **3l**, the potency decreased against CSF1R (Table 1) while the IC_{50} value against DAPK1 switched back to a similar level of compound **3h**.

In summary, we could successfully develop small molecules optimized for activity against both DAPK1 and CSF1R despite the known inherent difficulties in the optimization of a single molecule for activity against more than one target. The results show that the amide compounds

possessed promising dual inhibitory activity against both DAPK1 and CSF1R. Considering both targets, compound **3l** was the most potent compound achieved within this series.

2.4. Mechanism of DAPK1 and CSF1R inhibition

To identify the mode of action of the newly developed compounds as DAPK1/CSF1R dual inhibitors, a mechanistic study has been conducted for the most active member (compound **3l**) using three different concentrations of ATP (1, 10, and 100 μM).

2.4.1.Mechanism of DAPK1 inhibition

The impact of compound **3l**; the most potent DAPK1/CSF1R inhibitor on the phosphorylation of 20 μM concentration of the synthetic peptide substrate (KKLNRTLSFAEPG) by recombinant human DAPK1 (amino acids sequence 1-363) in presence of logarithmically increasing concentrations of ATP (1, 10, and 100 μM concentrations) was studied. The lowest ATP concentration was selected to be 1 μM which is close to the ATP K_m value for DAPK1 which is 1.24 μM concentration [36].

In contrast to the expected behavior of the typical ATP competitive kinase inhibitors whose elicited inhibition potency decreases with increasing the concentration of ATP, the dose-response curves (Figure 2) did not show a reduction of the measured inhibition for the kinase reaction upon increasing the ATP concentration. In addition, a slight enhancement of the measured IC_{50} was observed when ATP concentration was increased (IC_{50} values of 2.89, 1.25, and 0.92 μM when ATP concentrations were 1, 10, and 100 μM respectively). In other words, there was a proportional slight increase in the potency of compound **3l** with increasing the ATP concentration. The calculated K_i for inhibition of DAPK1 by compound **3l** was 0.581 μM.

Considering that the ATP K_m value for DAPK1 is 1.24 μM, compound **3l** might be a viable DAPK1 inhibitor at the cellular concentrations of ATP.

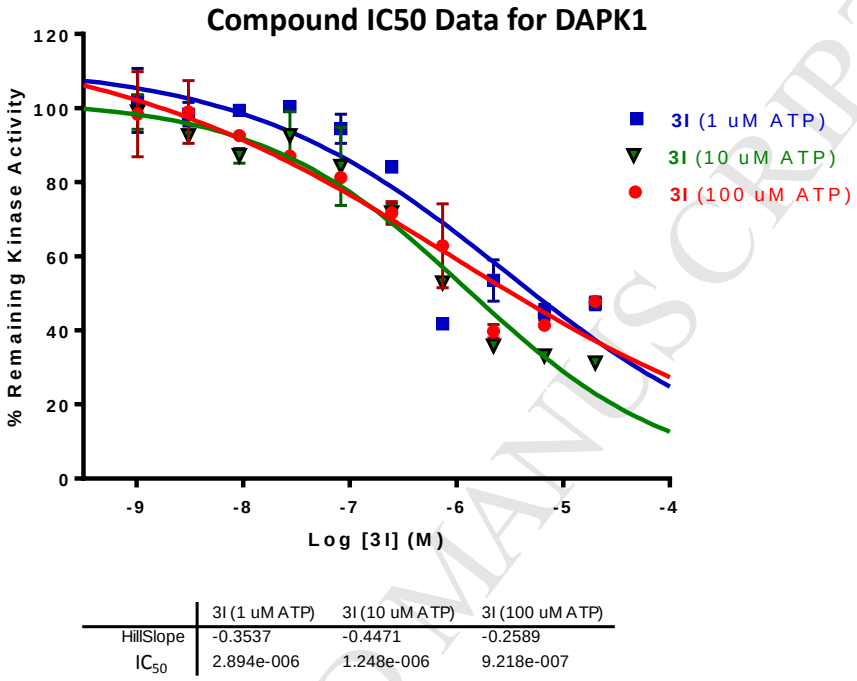

	3l (1 uM ATP)	3l (10 uM ATP)	3l (100 uM ATP)
HillSlope	-0.3537	-0.4471	-0.2589
IC_{50}	2.894e-006	1.248e-006	9.218e-007

Figure 2. Dose-response curves for the impact of compound **3l** on the kinase reaction of DAPK1 at 1, 10, and 100 μM concentrations of ATP.

As no competitive effect between ATP and compound **3l** was observed from the conducted study, it might be anticipated that compound **3l** is a non-ATP competitive inhibitor that binds to a site other than the ATP binding site of DAPK1. Furthermore, it seemed that ATP binding shifts conformational ensemble of DAPK1 to the conformational structure favored for binding of compound **3l**. Since no previous DAPK1 inhibitor has been reported to show a similar mode of inhibition, to the best of our knowledge, compound **3l** would be the first in its class as a non-ATP competitive DAPK1 inhibitor.

2.4.2.Mechanism of CSF1R inhibition

As compound **3l** was found to be non-ATP-competitive DAPK1 inhibitor, we addressed verification of its mechanism of inhibition of CSF1R. Accordingly, compound **3l** was assayed against CSF1R kinase at three different ATP concentration and the IC_{50} values were calculated. As shown in Figure 3, measured IC_{50} values of compound **3l** decreased as the ATP concentration increased (IC_{50} values of 0.069, 0.153, and 0.273 μM when ATP concentrations were 1, 10, and 100 μM respectively) and the calculated K_i for inhibition of DAPK1 by compound **3l** was 0.129 μM. This behavior might indicate that compound **3l** competes with ATP for the ATP pocket of CSF1R kinase. Accordingly, we might conclude that compound **3l** acts as ATP-competitive inhibitor of CSF1R although it might act as a non-ATP-competitive inhibitor for DAPK1.

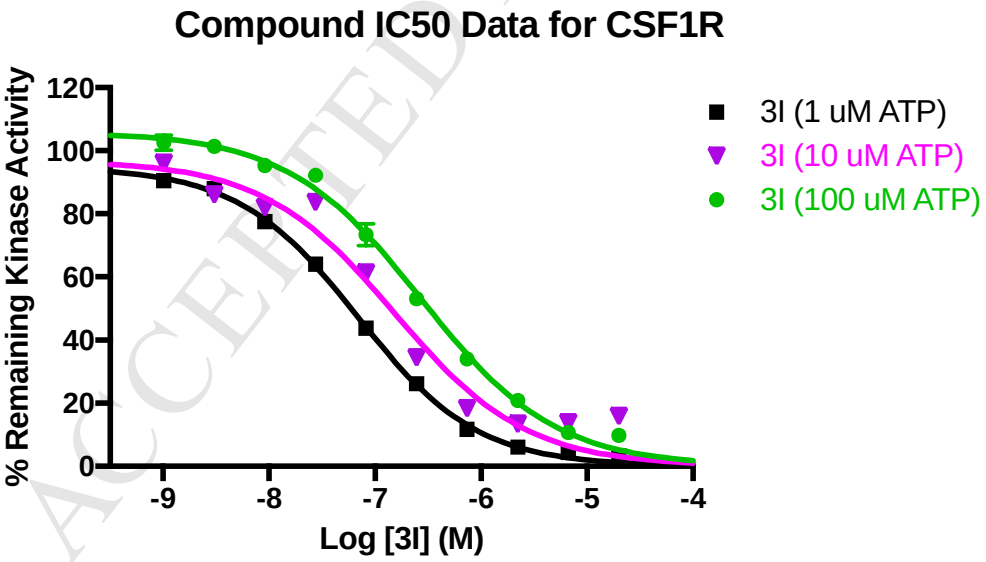

	3l (1 uM ATP)	3l (10 uM ATP)	3l (100 uM ATP)
HillSlope	-0.7701	-0.6986	-0.6879
IC_{50}	6.873e-008	1.533e-007	2.728e-007

Figure 3. Dose-response curves for the impact of **3l** on the CSF1R kinase reaction at 1, 10, and 100 μM concentrations of ATP.

2.5. *In vitro* cellular assays

2.5.1.Tau aggregation inhibition assay

As discussed in the introduction section, DAPK1 is involved in tau hyperphosphorylation, which is an essential step in the formation of tau aggregates. An *in vitro* active DAPK1 inhibitor should also be able to elicit a cellular activity manifested in the inhibition of the formation of tau aggregates to be considered a promising useful molecule for the targeting of tauopathies. Therefore, the urea compound **3b** and amide compounds (**3g–l**), which showed promising DAPK1 inhibitory activity, were evaluated at decreasing concentrations of 50, 10, and 1 μM using "tau Bimolecular Fluorescence Complementation assay" (tau-BiFC cell assay), which vitalizes tau aggregation in living HEK293 cell line [42, 43]. In the course of conduction of the assay, we followed the reported protocol using the same materials employing 30 μM concentration of forskolin as tau aggregation activator.

As shown in Figure 4, the results of the cellular assay showed that compound **3b**, which is the least potent DAPK1 inhibitor, as well as compound **3g**, which incorporate the lipophilic 3-(trifluoromethyl)phenyl moiety were ineffective at all of the used concentrations in the cellular assay for protection against the forskolin-induced tau aggregation. This cellular outcome for compound **3g** could possibly arise from a pharmacokinetic impact. For all other compounds (**3h–l**) possessing the relatively more hydrophilic methoxylated phenyl moieties, a variable degree of protection at 50 μM concentration was elicited. Among them, compound **3l** was the most effective in eliciting a complete protection against forskolin-induced tau aggregation at 50 μM

concentration. This matches with the *in vitro* conducted kinase assay, which revealed compound **3l** among all of the prepared compounds to possess the most potent IC_{50} against DAPK1. On the other hand, compound **3i**, which incorporates 3-methoxyphenyl moiety, showed the least efficient protection at 50 μM concentration which is also consistent with it low potency revealed from the conducted *in vitro* kinase assay against DAPK1. In addition to the potent compound **3l**, compounds **3h** and **3k** produced excellent protective activity at 50 μM concentration while compound **3j** produced an average protective activity. However, when the test concentration was decreased to 10 μM, only compound **3l** retained its excellent potency while compounds **3h** and **3k** showed almost a similar moderate protective activity. Consequently, compound **3l** was selected for further evaluation in 5-doses IC_{50} mode employing 1, 2, 4, 8 and 16 μM concentrations. The assay showed that compound **3l** elicited a cellular IC_{50} value of 5.0 μM while the 16 μM dose concentration almost completely protected against the forskolin-induced tau phosphorylation restoring it to the basal level. These results might indicate that the DAPK1 inhibitor compound **3l** could serve as a promising lead compound for the development of inhibitors of tau aggregates formation, and thus the development of promising tauopathies therapeutics.

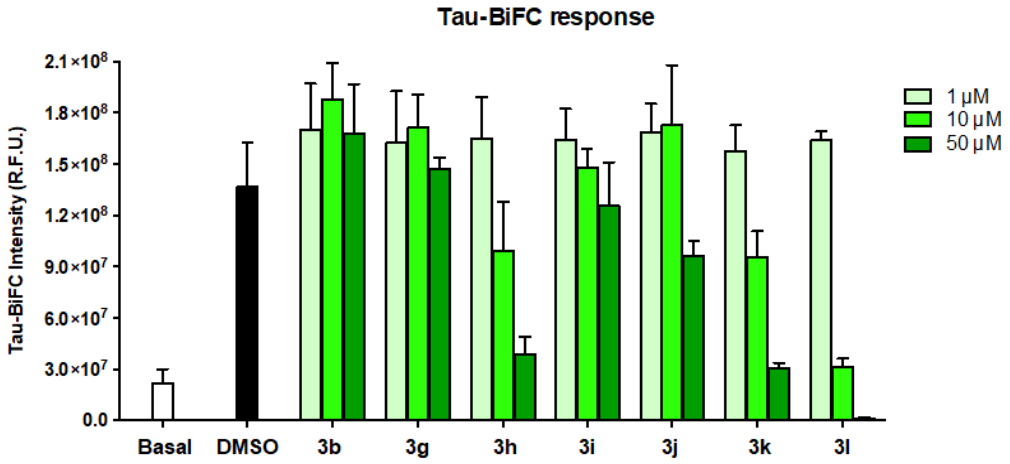

Figure 4. Effects of DAPK1 inhibitors on tau aggregation. HEK293 tau-BiFC cells were treated with each compound in various concentrations in the presence of forskolin (30 µM) for 48 h. Data are mean ± SD. The intensity of BiFC fluorescence was quantified by using a Harmony 3.1 software (PerkinElmer™).

2.5.2.*In vitro* anti-neuroinflammatory evaluation

The increased nitric oxide (NO) production is a major event in microglial neuroinflammation. In addition to its contribution to the increased hyperphosphorylation and formation of tau aggregates [44, 45], it also contributes to the neurodegenerative events by several mechanisms [46, 47]. Furthermore, it is interesting that nitration of tau protein has been identified in tauopathies [48, 49]. Moreover, NO produced from microglial neuroinflammation could lead to the formation of neurotoxic NO-dependent reactive nitrogen species (RNS) such as peroxynitrite [50, 51]. As we sought the development of multifunctional agents preventing both of formation of tau NFTs and neuroinflammation, it was important to evaluate the anti-neuroinflammatory activity of the compounds that showed promising protective activity against the formation of tau aggregates. Consequently, compound **3l** which showed the most potent activity in the tau-BiFC

cellular assay, as well as, compound **3h** which also elicited a good protective activity were selected for evaluation of anti-neuroinflammatory effects in the BV-2 microglial cell line. In addition, the *in vitro* kinase assay showed that these two compounds possess a submicromolar IC_{50} values activity against CSF1R. Accordingly, the lipopolysaccharides (LPS)-stimulated BV-2 cell line was used as a model for microglia-induced neuroinflammation to evaluate the effects of these two compounds [52].

As shown in Figure 5A, the 100 ng/mL concentration of LPS resulted in an abrupt increase of NO production in BV-2 cells. However, the presence of 10 μM concentration of compound **3l** attenuated the increased production of NO by around 55% of the production elicited by the positive control. This inhibition of LPS-induced NO production in microglia was highly significant ($p< 0.001$). As shown in Figure 5B the viability of BV-2 cells in the presence of both of compound **3l** and LPS was more than 92% of the control indicating that this reduction of NO production is due to specific inhibition of BV-2 cells by compound **3l**. However, a low inhibition percent for NO production was elicited by compound **3h** (Figure 5A) which was significant only at $p=0.1023$. It is worthy to mention that the structural difference between both compounds is only the N atom on the aromatic ring on position 2 of the pyrimidine ring. This structural difference resulted in the dramatic difference in cellular activity. Possibly, the introduction of the N atom to compound **3l** improved its physicochemical properties and allowed for a better cellular activity.

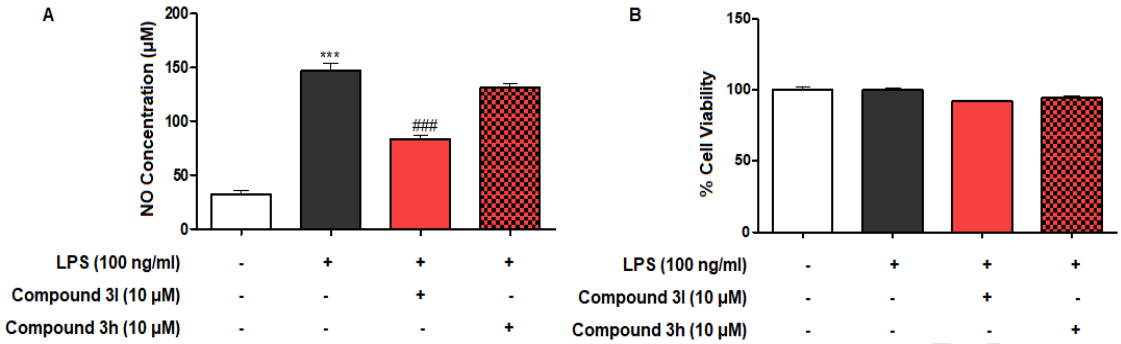

Figure 5. Effects of compounds **3h** and **3l** on LPS-induced BV-2 cell line. (A) Inhibition of NO production in LPS-stimulated BV-2 cell line by compounds **3h** and **3l**. Values are the means of five independent experiments ± SD. (B) the impact of for compounds **3h** and **3l** on the viability of BV-2 cell line. Values are the means of five independent experiments ± SD.

2.6. Selectivity profile

A considerable homology of the ATP-binding site between different kinases exists because kinases utilize the same natural molecule (ATP) as a ligand. As a result, the developed small molecule kinase inhibitor most likely inhibits more than one kinase. Consequently, selectivity is a major issue in developing kinase inhibitors to avoid off-target effects that may arise from the inhibition of kinases other than the targeted kinases. Accordingly, compound **3l**, which was revealed as a promising molecule targeting both of tau aggregation and of neuroinflammation, was subjected to kinase profiling to test its selectivity in inhibiting CSF1R and DAPK1 rather than other kinases. Even though the mechanistic study showed that **3l** does not compete with ATP for DAPK1, there is a possibility that it might bind the ATP pocket of other kinases as it was developed starting from ATP competitive inhibitors of CSF1R. In this regard, the selectivity was evaluated by profiling compound **3l** against a panel of 47 kinases. The panel included both DAPK1 and CSF1R family members in addition to other kinases representing diverse kinase

families. The profiling was performed via evaluating the percent inhibition produced by 10 μM concentration of compound **3l**.

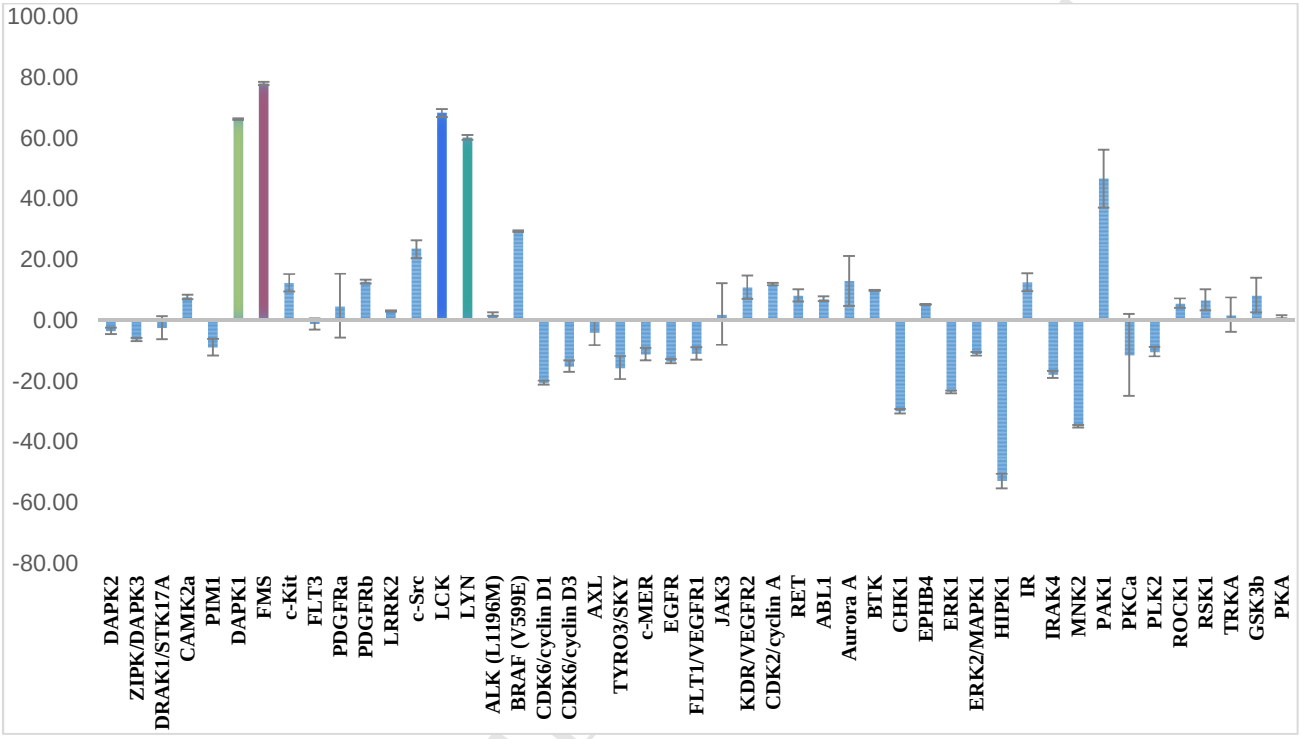

Figure 6. Selectivity profile elicited by 10 μM concentration of compound **3l** against a panel of 47 kinases including CSF1R and DAPK1. These data are the mean of two independent experiments ± standard deviation.

As shown in Figure 6, compound **3l** did not significantly inhibit most of the diverse kinases from the TK or STK families represented in the panel except for the expected inhibition of the src family members such as Lck, Lyn, and c-Src. In addition, compound **3l** did not inhibit other members of the PDGFR family arguing for a highly selective CSF1R inhibitor. Intriguingly, compound **3l** did not show any activity over DAPK2, DAPK3, and DRAK1 kinases despite the high sequence homology between the kinase domains of DAPK1, DAPK2, and DAPK3 (more

than 80% sequence homology in their kinase domains). It also did not show any activity against other related kinases such as PIM1, LRRK2 or CaMK2a suggesting that compound **3l** is highly selective towards CSF1R and DAPK1.

To the best of our knowledge, none of the known DAPK1 inhibitors reached this level of selectivity within the DAPK family with preferential selectivity for DAPK1 over the other family members. The results obtained from the mechanistic study and the observed subtype selectivity within the DAPK family suggest that compound **3l** binds to another binding site other than the ATP-binding site arguing for a potential first-in-class non-ATP-competitive inhibitor of DAPK1. In summary, compound **3l** showed high selectivity for DAPK1 and CSF1R against other members of the DAPK or PDGFR families.

2.7. Cardiac safety profile (*In vitro* Predictor™ hERG Fluorescence Polarization Assay)

Early assessment of the potential cytotoxicity is important to minimize the risk of failure of drug discovery programs [53]. The human Ether-a-go-go-Related Gene (hERG aka KCNH2) is a gene that encodes for two voltage-gated potassium channels [54]. The hERG potassium channels are involved in action potential repolarization in the heart [55]. Both inhibition and activation of hERG channels by non-cardiovascular drugs are considered as a severe toxic effect that should be eliminated early in the drug development process [56]. In fact, several drugs have been dropped after marketing because of their significant cardiotoxic effects due to their off-target effect on the hERG channels [57]. Consequently, the promising compound **3l** was evaluated against the hERG channel in a 10-dose IC_{50} mode starting at 100 μM with 3-fold serial dilution employing Predictor™ hERG Fluorescence Polarization Assay. The assay uses a membrane

containing hERG channel protein and a high-affinity fluorescent hERG channel ligand (Tracer). The ability of the test compound to compete with the tracer for the hERG binding reflects the ability of the test compound to inhibit the hERG channel. Compound **3l** showed good cardiac safety profile with an *in vitro* IC_{50} value of 17.1 μM against hERG channel (Table 2). This result suggests that compound **3l** does not elicit significant cardiotoxicity and therefore, a suitable lead compound for further development.

Table 2. hERG channel affinity data (as IC_{50} value) of compound **3l**.

Compd.	IC_{50} of tracer binding (μM) against hERG [a]	P_e (10^{-6} Cm/sec) ± SD
3l	17.1	57.0 ± 3.3 [b]
E-4031 [c]	0.01	ND [d]
Progesterone [e]	ND	33.3 ± 0.7
Theophylline [f]	ND	0.26 ± 0.06

[a] The compound was tested in a singlicate 10-dose IC_{50} mode starting at 100 μM with 3-fold serial dilution.
[b] The compound was tested using 12.5 μM concentration and the results shown are the means of three independent experiments ± standard deviation.
[c] E-4031 is the positive control agent for the hERG channel assay.
[d] ND: Not determined
[e] Progesterone (50 μM) was used as the positive control agent for the PAMPA assay.
[f] Theophylline (50 μM) was used as the negative control agent for the PAMPA assay.

2.8. Blood-Brain Barrier (BBB) penetration evaluation (PAMPA assay)

The ability of CNS-directed therapeutic agents to cross the BBB determines the effectiveness of these agents *in vivo* and minimize the potential peripheral side effects that result from poor BBB penetration. Since our designed compounds target DAPK1 and CSF1R for management of tauopathies, it was essential to assess their ability to cross the BBB. For that, we have selected the most potent member of our series (**3l**) to be evaluated using the parallel artificial membrane

permeability assay (PAMPA) [58]. The PAMPA assay uses BBB-PAMPA lipid membrane and measures the ability of a certain chemical to cross this membrane and therefore measures its effective permeability (P_e) (detailed experimental protocol is discussed in the experimental section). In order to evaluate the obtained P_e values, certain standards were applied. If the P_e is more than 0.4 (10^{-6} cm/sec), the tested compound is considered as highly permeable and if it is more than 10 (10^{-6} cm/sec), the compound is considered as highly CNS bioavailable. Progesterone (high BBB-penetrating drug) was used as a positive control and showed P_e (± SD values) value of 33.3 ± 0.7 while theophylline (low BBB-penetrating drug) was used as negative control and showed P_e value of 0.26 ± 0.06. When compound **3l** was assayed at the same conditions, it showed P_e value of 57.0 ± 3.3 accounting for around 71% higher penetration ability than the positive control (Table 2). These results suggest that compound **3l** could have high BBB penetration and high CNS bioavailability and is a suitable lead for further development.

2.9. *In silico* molecular simulation study

In order to identify the binding mode and receptor interactions of this new class of DAPK1/CSF1R inhibitors, a molecular docking study was performed. The crystal structures of the catalytic kinase domain of DAPK1 (PDB code: 4TXC; Figure 7) and CSF1R kinase domain (PDB code: 3KRJ) were used for the docking study employing SwissDock which is based on the docking software EADock DSS running on the Vital-IT cluster [59]. Docking was performed in the accurate mode as a blind docking study where binding modes are generated in the vicinity of all cavities of the used structure. Simultaneously, their CHARMM energies were estimated on a grid. The binding modes with the most favorable energies were evaluated with FACTS and clustered and visually inspected [60].

2.9.1.Docking results to DAPK1

The results of the conducted *in silico* blind docking showed that this class of compounds might dock within two pockets only in the employed structure of DAPK1, the ATP-binding pocket and another pocket which was identified as the protein substrate-binding site [61].

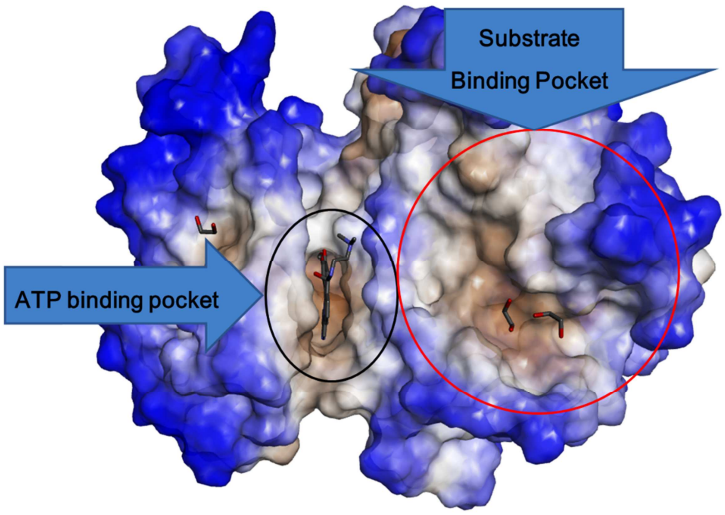

Figure 7. The ATP-binding site and the substrate-binding sites of the DAPK1 protein. A hydrophobic surface was generated around the protein using Discovery studio program standard protocol for surface generation.

In the case of compound **3l**, which is the most potent compound among the prepared series, the calculations predicted that the best-docked pose is within the substrate-binding pocket (Figure 8A). This binding mode for compound **3l** showed a high overall favorable free energy (ΔG = -9.21 kcal/mol). Several polar and hydrophobic interactions of compound **3l** within the substrate-binding site contributed to the stabilization of this binding mode. Thus, the 3,5-

dimethoxybenzoyl group docked into the hydrophobic pocket eliciting interactions with Leu111, Lys108, and Ala106. The carbonyl group of the amide established a hydrogen bond with the backbone NH group of Leu111. The NH group at position 2 of the pyrimidine core interacted with the Glu113 side chain. The morpholine was directed to the solvent exposure region while the *p*-methoxyphenyl interacted with Asn243 and Glu239. On the other hand, the best scoring pose of compound **3l** within the ATP-binding site showed a relatively lower score (ΔG = -8.36 kcal/mol) and, more importantly, was unable to establish the crucial interactions with key residues within the hinge region (Figure 8B). It showed a flipped binding mode in which the dimethoxyphenyl moiety docked into the hydrophobic pocket showing interactions with Leu19, Val27, Ala40, Glu94, and Ile160. The pyrimidine ring interacted with Lys42 and Asp161. While the morpholine was directed to the solvent and the phenyl group carrying the morpholine interacted with Gln23. The methoxyphenyl moiety interacted with the peptide bond between Gly20 and Ser21. Together, these results indicate that compound **3l** might act through binding to the substrate-binding site rather than the ATP binding pocket of DAPK1.

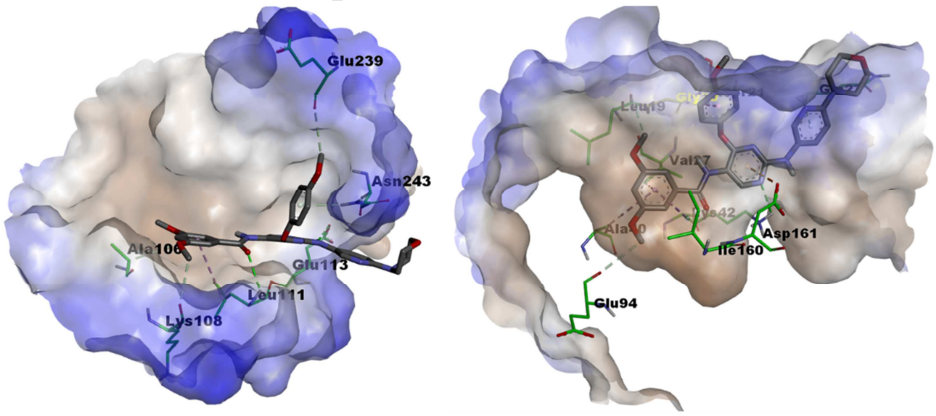

Figure 8. *In silico* calculated binding modes of compound **3l** within DAPK1. (A) Calculated binding mode of **3l** within the substrate-binding site of DAPK1. (B) Calculated binding mode of **3l** within the ATP-binding site of DAPK1.

Considering the case of compound **3g**, which is a less potent DAPK1 inhibitor, a score lower than that for compound **3l** was calculated for the docked pose within the substrate-binding site (ΔG = -8.92 kcal/mol for compound **3g** while ΔG = -9.21 kcal/mol for compound **3l**). This could explain the relative potencies of these compounds. The calculated binding mode within the substrate-binding site showed slight deviation in the orientation of compound **3g** relative to that of compound **3l** (Figure 9A). In this binding mode of compound **3g**, the 3-trifluoromethylphenyl moiety docked into the hydrophobic pocket showing interactions with Phe102, Leu105, Ala106, Ile209, and Leu210. Meanwhile, the pyrimidine ring interacted with Leu111, Ala116, and Leu210. The morpholine was directed to solvent exposure. The amide NH interacted with Leu210. Considering the *in silico* prediction for possible binding of compound **3g** within the ATP-binding site, the calculated pose showed a higher score (ΔG = -9.23 kcal/mol) than that within the substrate-binding site but missed the crucial interactions with key residues of the hinge region (Figure 9B). In this calculated pose, the 4-methoxyphenyl ring fitted into the hydrophobic pocket showing interactions with Val27, Lys42, Glu64, Leu93, Ile160, and Asp161, while the pyrimidine ring interacted with Val27. The morpholine was directed to solvent exposure while the phenyl group carrying the morpholine interacted with Leu19 and Met146. The trifluoromethyl interacted with Phe24 and Ala25 while the phenyl group carrying the trifluoromethyl moiety interacted with Ala25 and Asp161. Despite the higher score of the pose of compound **3g** within the ATP pocket than within the substrate-binding pocket, lacking

interactions with the key residues of the hinge region may exclude this binding mode from our consideration. In addition, the similarity of orientation and interaction patterns of the best pose of compound **3g** with that of the most active compound **3l** within the substrate-binding pocket supports that DAPK1 inhibition by compounds **3g** might be also mediated through binding to the substrate-binding pocket.

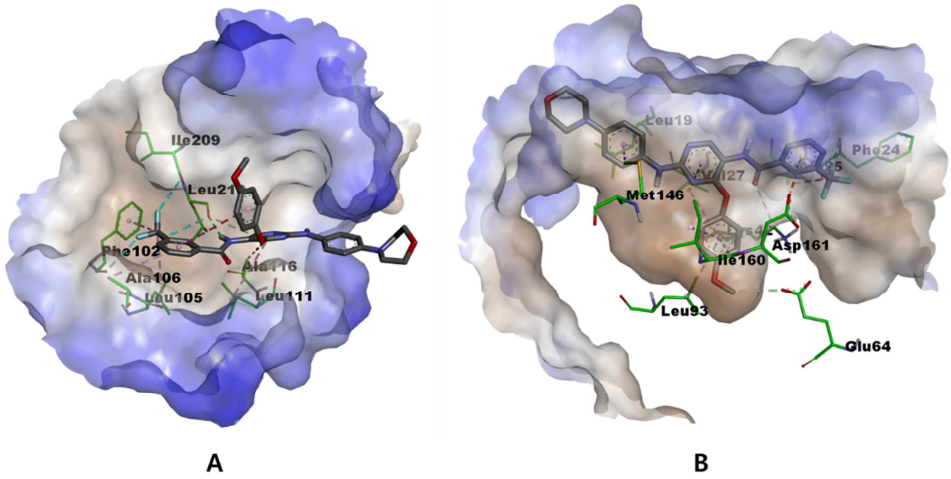

Figure 9. *In silico* calculated binding modes of compound **3g** within DAPK1. A) Calculated binding mode of **3g** within the substrate-binding site of DAPK1. B) Calculated binding mode of **3g** within the ATP-binding site of DAPK1.

Collectively, the results of the *in silico* conducted study were consistent with what has been revealed from the mechanistic study that this class of compounds does not fit properly in the ATP-binding site of DAPK1. In addition, it suggests that this class of compounds acts as protein-protein interactions inhibitors (PPI-inhibitors) via binding to the substrate binding site of DAPK1 and thus blocks the access of the protein substrates resulting in inhibition of kinase reaction of

DAPK1. This would also explain the high selectivity of compound **3l** for inhibiting only DAPK1 among other members of the DAPK family of protein kinases and other related kinases.

2.9.2.Docking results to CSF1R

Because the conducted mechanistic study of compound **3l** indicated that its mechanism for CSF1R inhibition is different from that for DAPK1 inhibition, we conducted a molecular docking study of compound **3l** to CSF1R. In contrast to the results of the conducted blind docking study to DAPK1, herein, the results showed that compound **3l** docked within ATP pocket of CSF1R but not in other site(s). This result is in agreement with the results of the conducted mechanistic study of compound **3l**.

Investigation of the top ten poses should that the 3,5-dimethoxyphenyl moiety in the top six retrieved poses as well as pose No. 9 docked into the hydrophobic pocket (Figure 10), which is a binding mode different from the previously predicted for compound **2** in our previous report which predicted that the morpholino moiety docked deep into the binding pocket and the moiety3,5-dimethoxyphenyl moiety projected outside. Among poses 1–6 and 9, binding to Tyr665 (hinge region) was detected only in poses No. 3 and 9. Only in pose No 10 the morpholine ring was docked into the hydrophobic pocket similar to compound **2**. However, in this pose, it showed no interaction with Tyr665 (hinge region). In poses No. 7 and 8, the 4-methoxyphenoxy moiety was docked into the hydrophobic pocket. However, in both poses 7 and 8, there was no interaction with Tyr665 (hinge region). This could possibly rationalize the lower inhibition potency against CSF1R observed in this series relative to that of compound **2**. In addition, these docking study results further supports our finding that **3l** inhibits CSF1R kinase through an ATP-competitive mechanism.

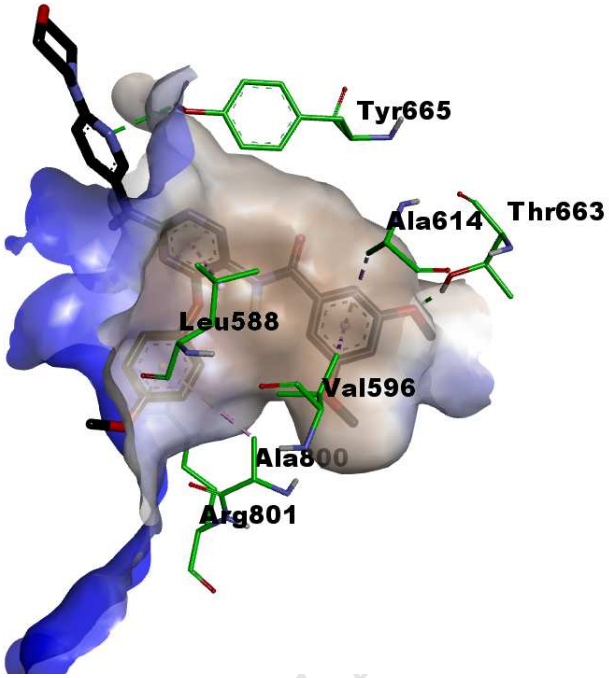

Figure 10. *In silico* calculated binding modes of compound **3l** within the ATP pocket of the CSF1R kinase (pose No. 3) showing regular binding mode with the 3,5-dimethoxyphenyl moiety embedded deep inside the hydrophobic pocket of the ATP binding site.

3. Conclusion

In the course of searching for and developing novel promising therapeutics for tauopathies (a group of complex neurodegenerative diseases), this study aimed to design and evaluate small molecules dual inhibitors of DAPK1 and CSF1R kinases. By inhibiting both kinases, we aimed at targeting both the formation of tau neurofibrillary tangles and the neurodegeneration-associated neuroinflammation which are two major components of tauopathies. In this regard, this work used our recently developed CSF1R inhibitor (compound **2**) as a starting point. Guided by the chemical structure of a recently reported ATP-competitive DAPK1 inhibitor (compound

1) the structure of compound **2** was modified in attempts to obtain small molecules capable of inhibiting both of DAPK1 and CSF1R. *In vitro* evaluation of the inhibition of DAPK1 and CSF1R kinase reactions by the prepared compounds showed that the amide derivative (**3g–l**) gained significant inhibitory activity against DAPK1 and retained excellent inhibitory activity against CSF1R. In contrast, urea compounds (**3a–f**) did not gain sufficient inhibitory activity against DAPK1 and/or lost potential activity against CSF1R. To verify the type of the newly developed DAPK1/CSF1R inhibitors, a mechanistic study was conducted using logarithmically increasing concentrations of ATP (1, 10 and 100 μM concentrations) for the most potent member, compound **3l**. The results indicated that these inhibitors are potential non-ATP-competitive DAPK1 inhibitors but they compete with ATP for CSF1R kinase.

To assess the potentiality of these compounds to inhibit the formation of tau protein aggregates, the tau-BiFC cellular assay was performed which revealed a good to an excellent cellular activity of compounds **3h**, **3k**, and **3l**. The IC_{50} was measured to be 5.0 μM for compound **3l**, which was the most potent compound in the cellular assay. To assess the dual functionality of the developed molecules against neuroinflammation and formation of tau aggregates, compound **3l**, which was the most potent inhibitor for formation of tau-aggregates, as well as, compounds **3h** which elicited good activity in the tau-BiFC assay were further evaluated for inhibition of the production of NO in LPS-induced BV-2 microglial cell line as a model for microglial neuroinflammation. Pleasantly, compound **3l** inhibited the stimulated production of NO by around 55% indicating that it might act as dual-functional molecule counteracting both the neuroinflammation and the tau-aggregation into NFTs.

To assess the probability of off-target effects that might arise from inhibition of other kinases by compound **3l**, kinase profiling was performed against a panel of 47 kinases representing

diverse kinases' families and including other members of the DAPK family and related members. The results revealed high selectivity of compound **3l** for DAPK1 and CSF1R over other kinases included in the screened panel. Furthermore, an exclusive selectivity for DAPK1 over the other members of DAPK family and related kinases was observed which might be attributed to the unique mechanism of DAPK1 inhibition by compound **3l**. For further assessment of compound **3l** safety, *in vitro* "Predictor™ hERG fluorescence polarization assay" was conducted as a measurement for potential cardiotoxicity. The assay showed a good cardio safety profile for compound **3l**. In addition, compound **3l** was predicted to have a high CNS penetration and bioavailability using PAMPA-BBB assay. To predict the possible binding site of these compounds within DAPK1, a blind docking study was conducted. The *in silico* calculations showed that these compounds might not dock properly within the ATP-pocket which is consistent with the performed mechanistic study. Instead, the *in silico* study predicted these compounds to dock within the substrate-binding site suggesting that these compounds might act as small molecule PPI inhibitors blocking the access of the substrates to the substrate-binding site of DAPK1, thus, hindering binding of the substrate to the DAPK1 which is a crucial step of the kinase reaction. On the other hand, **3l** was docked inside the ATP pocket of CSF1R in the retrieved poses further supporting the mechanistic study results.

In summary, this work presents compound **3l** as a unique, effective and selective inhibitor of both DAPK1 and CSF1R. The activity and safety of compound **3l** have been proven *in vitro* and in cellular assays while the mechanism of DAPK1 inhibition has been studied *in vitro* and *in silico*. Compound **3l** could serve as a promising lead compound for further development of novel anti-tauopathy and/or anti-neuroinflammatory therapies.

4. Experimental

4.1. Chemistry

4.1.1.General

All reactions and manipulations were carried out using standard Schlenk techniques. The starting materials, reagents, and solvents were purchased from commercial suppliers and were used as purchased. All melting points were measured by Optimelt Automated Melting Point System (Stanford Research Systems) and are uncorrected. Thin-layer chromatography was performed with Merk silica gel 60 F_{254} pre-coated glass sheets. Column chromatography was performed on Merck Silica Gel 60 (230-400 mesh) or by using Biotage Isolera One flash chromatography system and the eluting solvents are noted as a mixed solvent with given volume-to-volume ratios or as a percentage. ^{1}H & ^{13}C NMR was measured on a 400 MHz Bruker Avance NMR spectrometer. Chemical shifts and coupling constants are presented in parts per million (ppm) relative to Me_4Si and hertz (Hz), respectively, and the following abbreviations are used: s, singlet; d, doublet; dd, a doublet of doublets; t, triplet; m, multiplet. High-resolution mass spectra were performed on Waters ACQUITY UPLC BEH C18 1.7µ−Q-TOF SYNAPT G2-Si High Definition Mass Spectrometry.

4.1.2.General procedure for preparation of 5a–f

The procedure for preparation of **5a–f** was followed as reported and compounds **5a**, **5e,** and **5f** were prepared as previously reported [37].

4-(4-methoxyphenoxy)-N-(6-morpholinopyridin-3-yl)-5-nitropyrimidin-2-amine (5b)

Orange solid, yield 50%, mp: 217.1–218.9 °C. ^{1}H NMR (400 MHz, DMSO-d_6): δ10.60 (s, 1H), 9.13 (s, 1H), 8.02 (d, 1H, *J* = 2.2 Hz), 7.41 (dd, 1H, *J* = 9.0, 2.3 Hz), 7.19 (d, 2H, *J* = 8.9 Hz), 7.04 (d, 2H, *J* = 8.9 Hz), 6.41 (d, 1H, *J* = 9.2 Hz), 3.81 (s, 3H), 3.69 (t, 4H, *J* = 4.6 Hz), 3.32 (s, 4H); ^{13}C NMR (100 MHz, DMSO-d_6): δ 163.60, 159.73, 158.86, 157.75, 156.10, 145.55, 140.21, 130.55, 126.60, 123.71, 123.37, 123.20, 115.22, 106.18, 66.33, 55.95, 45.81; HRMS (ES^+): *m/z* calculated for $C_{20}H_{20}N_6O_5$: 447.1393 $[M+Na]^+$. Found 447.1395.

N-(4-fluorophenyl)-4-(4-methoxyphenoxy)-5-nitropyrimidin-2-amine (5c)

Greenish yellow solid, yield 78.5%, mp: 219.0–220.1 °C. ^{1}H NMR (400 MHz, DMSO-d_6): δ 10.70 (s, 1H), 9.17 (s, 1H), 7.29–7.23 (m, 4H), 7.09 (d, 2H, *J* = 7.8 Hz), 6.82 (s, 2H), 3.84 (s, 3H); ^{13}C NMR (100 MHz, DMSO-d_6): δ 163.10, 159.11, 158.34, 157.22, 156.75, 145.12, 134.60, 123.57, 122.97, 121.44, 114.69, 114.50, 55.50.

4-(4-methoxyphenoxy)-5-nitro-N-(6-(piperidin-1-yl)pyridin-3-yl) pyrimidin-2-amine (5d)

Yellow solid, yield 40.8%, mp: 189.9–190.9 °C. ^{1}H NMR (400 MHz, $CDCl_3$): δ 9.10 (s, 1H), 7.89 (s, 1H), 7.64 (s, 1H), 7.29 (d, 1H, *J* = 9.0 Hz), 7.08 (d, 2H, *J* = 8.8 Hz), 6.96 (d, 2H, *J* = 9.0 Hz), 6.25 (d, 1H, *J* = 9.1 Hz), 3.86 (s, 3H), 3.51–3.45 (m, 4H), 1.63 (s, 6H); ^{13}C NMR (100 MHz, DMSO-d_6): δ 163.62, 159.70, 158.87, 157.74, 156.09, 145.58, 140.33, 130.68, 125.39, 123.61, 123.41, 123.22, 115.23, 106.02, 55.93, 46.26, 25.29, 24.73.

4.1.3.General procedure for preparation of 6a–f

The procedure for preparation of **6a–f** was followed as reported and compounds **6a, 6e,** and **6f** were prepared as previously reported [37].

4-(4-methoxyphenoxy)-N^2-(6-morpholinopyridin-3-yl)pyrimidine-2,5-diamine (6b)

Yellow solid darkens to deep blue, yield 100%, mp: 198.9–200.9 °C. ^{1}H NMR (400 MHz, DMSO-d_6): δ 8.58 (s, 1H), 8.21 (d, 1H, *J* = 2.6 Hz), 7.81 (s, 1H), 7.69 (dd, 1H, *J* = 9.0, 2.6 Hz), 7.14 (d, 2H, *J* = 9.0 Hz), 7.00 (d, 2H, *J* = 9.0 Hz), 6.55 (d, 2H, *J* = 9.1 Hz), 4.54 (s, 2H), 3.79 (s, 3H), 3.68 (t, 4H, *J* = 4.5 Hz), 3.25 (t, 4H, *J* = 4.7 Hz).

N^2-(4-fluorophenyl)-4-(4-methoxyphenoxy)pyrimidine-2,5-diamine (6c)

Yellow solid darkens to deep blue, yield 100%, mp: 193.3–195.0 °C. ^{1}H NMR (400 MHz, DMSO-d_6): δ 8.88 (s, 1H), 7.85 (s, 1H), 7.45–7.40 (m, 2H), 7.16 (d, 2H, *J* = 9.0 Hz), 7.03 (d, 2H, *J* = 9.4 Hz), 6.85–6.81 (m, 2H), 4.62 (s, 2H), 3.80 (s, 3H); ^{13}C NMR (100 MHz, DMSO-d_6): δ 158.55, 157.64, 157.02, 155.30, 151.52, 146.56, 142.96, 138.38, 138.36, 123.51, 123.37, 118.95, 118.88, 116.17, 115.05, 115.00, 114.96, 114.74, 55.97.

4-(4-methoxyphenoxy)-N^2-(6-(piperidin-1-yl)pyridin-3-yl)pyrimidine-2,5-diamine (6d)

Yellow solid darkens to deep blue, yield 99.3%, mp: 178.4–180.4 °C. ^{1}H NMR (400 MHz, DMSO-d_6): δ 8.51 (s, 1H), 8.15 (d, 1H, *J* = 2.6 Hz), 7.80 (s, 1H), 7.61 (dd, 1H, *J* = 9.1, 2.8 Hz), 7.14 (d, 2H, *J* = 9.0 Hz), 7.00 (d, 2H, *J* = 9.0 Hz), 6.52 (d, 1H, *J* = 9.1 Hz), 4.52 (s, 2H), 3.79 (s, 3H), 3.34–3.32 (m, 4H), 1.53 (s, 6H); ^{13}C NMR (100 MHz, DMSO-d_6): δ 158.76, 156.93, 154.83, 154.78, 152.57, 152.24, 151.58, 146.54, 146.37, 143.11, 138.30, 129.71, 129.45, 129.16,

128.95, 123.36, 122.88, 116.17, 115.06, 115.00, 107.39, 106.92, 55.90, 46.91, 25.46, 25.40, 24.76.

4.1.4.General procedure for preparation of 3a–f [62]

To a solution of compounds **6a–f** (0.1 mmol) in glacial acetic acid (2 mL) was added an aqueous solution of potassium cyanate (0.2 mmol in 1 mL water), dropwise. The reaction mixture was stirred at rt for 2 h at which TLC indicated total consumption of the starting amine. The mixture was then diluted with water and extracted with EA (3 x 5 mL). The organic layer was dried over anhydrous sodium sulfate and evaporated. The residue was purified by column chromatography.

1-(4-(4-methoxyphenoxy)-2-((4-morpholinophenyl)amino)pyrimidin-5-yl)urea (3a)

Yellowish white solid, yield 45.8%, mp: 243.9–245.2 °C. ^{1}H NMR (400 MHz, DMSO-d_6): δ 9.04 (s, 1H), 8.69 (s, 1H), 8.05 (s, 1H), 7.27 (d, 2H, *J* = 8.3 Hz), 7.18 (d, 2H, *J* = 8.6 Hz), 7.03 (d, 2H, *J* = 8.5 Hz), 6.64 (d, 2H, *J* = 8.6 Hz), 6.14 (s, 2H), 3.81 (s, 3H), 3.71 (s, 4H), 2.95 (s, 4H); ^{13}C NMR (100 MHz, DMSO-d_6): δ 160.36, 156.63, 156.24, 154.32, 150.32, 145.72, 145.32, 133.24, 123.08, 119.02, 115.31, 114.49, 113.27, 66.04, 55.37, 49.27; HRMS (ES^+): m/z calculated for $C_{22}H_{24}N_6O_4$: 459.1757 $[M+Na]^+$. Found 459.1751.

1-(2-((4-morpholinophenyl)amino)-4-(4-(trifluoromethyl)phenoxy)pyrimidin-5-yl)urea (3b)

White solid, yield 69.5%, mp: 263.1–265.0 °C. ^{1}H NMR (400 MHz, DMSO-d_6): δ 9.16 (s, 1H), 8.74 (s, 1H), 8.03 (s, 1H), 7.89 (d, 2H, *J* = 8.5 Hz), 7.52 (d, 2H, *J* = 8.4 Hz), 7.18 (d, 2H, *J*

= 8.7 Hz), 6.60 (d, 2H, *J* = 8.9 Hz), 6.11 (s, 2H), 3.71 (t, 4H, *J* = 4.9 Hz), 2.92 (t, 4H, *J* = 4.6 Hz); ^{13}C NMR (100 MHz, DMSO-d_6): δ159.89, 156.18, 155.73, 154.35, 151.50, 145.46, 132.90, 126.98, 126.94, 126.08, 125.76, 125.46, 123.29, 122.76, 119.09, 115.17, 113.18, 65.99, 49.14; HRMS (ES$^+$): m/z calculated for $C_{22}H_{21}F_3N_6O_3$: 497.1525 $[M+Na]^+$. Found 497.1528.

1-(4-(3-methoxyphenoxy)-2-((4-morpholinophenyl)amino)pyrimidin-5-yl)urea (3c)

Yellowish white solid, yield 81.2%, mp: 206.2–207.9 °C. ^{1}H NMR (400 MHz, DMSO-d_6): δ 9.08 (s, 1H), 8.72 (s, 1H), 7.97 (s, 1H), 7.40 (t, 1H, *J* = 8.1 Hz), 7.30 (d, 2H, *J* = 9.0 Hz), 6.92–6.82 (m, 3H), 6.65 (d, 2H, *J* = 9.0 Hz), 6.10 (s, 2H), 3.77 (s, 3H), 3.71 (t, 4H, *J* = 4.4 Hz), 2.95 (t, 4H, *J* = 4.6 Hz); ^{13}C NMR (100 MHz, DMSO-d_6): δ 172.58, 160.85, 160.51, 156.77, 154.97, 154.06, 151.20, 145.99, 133.80, 130.55, 119.92, 119.59, 115.92, 114.72, 113.95, 111.69, 108.68, 66.64, 55.89, 49.87; HRMS (ES$^+$): m/z calculated for $C_{22}H_{24}N_6O_4$: 437.1937 $[M+H]^+$. Found 437.1938.

1-(2-((4-fluorophenyl)amino)-4-(4-methoxyphenoxy)pyrimidin-5-yl)urea (3d)

White solid, yield 80%, mp: 278.0–280.0 °C. ^{1}H NMR (400 MHz, Acetone-d_6): δ 8.95 (s, 1H), 7.56–7.52 (m, 2H), 7.36 (s, 2H), 7.17 (d, 2H, *J* = 8.8 Hz), 7.05 (d, 2H, *J* = 8.9 Hz), 6.85 (t, 2H, *J* = 8.8 Hz), 3.88 (s, 3H); ^{13}C NMR (100 MHz, DMSO-d_6): δ 160.67, 157.30, 156.68, 154.38, 150.33, 146.21, 137.60, 123.67, 119.81, 119.73, 115.12, 115.04, 114.82, 114.70, 56.00; HRMS (ES$^+$): m/z calculated for $C_{18}H_{16}FN_5O_3$: 370.1315 $[M+H]^+$. Found 370.1323.

1-(4-(4-methoxyphenoxy)-2-((6-morpholinopyridin-3-yl)amino)pyrimidin-5-yl)urea (3e)

White solid, yield 50%, mp: 212.0–213.6 °C. ^{1}H NMR (400 MHz, MeOH-d_4): δ 8.53 (s, 1H), 8.08 (d, 1H, *J* = 2.6 Hz), 7.66 (dd, 1H, *J* = 9.0, 2.7 Hz), 7.10 (d, 2H, *J* = 9.0 Hz), 6.98 (d, 2H, *J* = 9.0 Hz), 6.54 (d, 2H, *J* = 9.1 Hz), 3.83 (s, 3H), 3.78 (t, 4H, *J* = 4.7 Hz), 3.34–3.31 (m, 4H); ^{13}C NMR (100 MHz, MeOH-d_4): δ 164.01, 160.12, 158.91, 157.60, 157.10, 147.52, 140.08, 131.87, 130.52, 124.16, 115.72, 114.11, 108.59, 67.84, 56.22; HRMS (ES^+): m/z calculated for $C_{21}H_{23}N_7O_4$: 438.1890 $[M+H]^+$. Found 438.1896.

1-(4-(4-methoxyphenoxy)-2-((6-(piperidin-1-yl)pyridin-3-yl)amino)pyrimidin-5-yl)urea (3f)

White solid, yield 98%, mp: 213.6–214.2 °C. ^{1}H NMR (400 MHz, MeOH-d_4): δ 8.51 (s, 1H), 8.01 (d, 1H, *J* = 2.5 Hz), 7.60 (dd, 1H, *J* = 9.1, 2.7 Hz), 7.10 (d, 2H, *J* = 9.0 Hz), 7.00 (d, 2H, *J* = 9.0 Hz), 6.52 (d, 1H, *J* = 9.2 Hz), 3.83 (s, 3H), 3.37 (s, 4H), 1.63 (s, 6H); ^{13}C NMR (100 MHz, MeOH-d_4): δ 164.07, 160.13, 158.87, 157.73, 157.49, 153.67, 147.50, 140.09, 132.25, 129.38, 124.14, 123.45, 115.67, 113.91, 108.95, 56.18, 26.59, 25.71; HRMS (ES^+): m/z calculated for $C_{22}H_{25}N_7O_3$: 436.2097 $[M+H]^+$. Found 436.2099.

4.1.5.General procedure for preparation of 3g–l

To a solution of compound **6a–d** (0.1 mmol) in DCM (3 mL) was added DIPEA (0.15 mmol) and the solution was cooled to –78 °C using acetone/dry ice bath. To this cold solution was added an ice-cooled solution of appropriate acid chloride (0.1 mmol) in 2 mL DCM, dropwise. The acetone/dry ice bath was removed and the reaction mixture was allowed to warm to room temperature and stirred for 2 h (TLC checked). Upon reaction completion, the reaction mixture

was evaporated and the crude product was purified by column chromatography using EA: hexane mixtures.

N-(4-(4-methoxyphenoxy)-2-((4-morpholinophenyl)amino)pyrimidin-5-yl)-3-(trifluoromethyl)benzamide (3g)

White solid, yield 23%, mp: 169.5–171.5 °C. ^{1}H NMR (400 MHz, $CDCl_3$): δ 9.21 (s, 1H), 8.20 (s, 1H), 8.09 (d, 1H, *J* = 7.7 Hz), 8.00 (s, 1H), 7.83 (d, 1H, *J* = 7.8 Hz), 7.65 (t, 1H, *J* = 7.8 Hz), 7.26–7.23 (m, 3H), 7.13 (d, 2H, *J* = 9.0 Hz), 7.00 – 6.96 (m, 2H), 6.90 (s, 1H), 6.74 (d, 2H, *J* = 9.0 Hz), 3.87–3.84 (m, 7H), 3.07 (t, 4H, *J* = 4.8 Hz); ^{13}C NMR (100 MHz, $CDCl_3$): δ 157.45, 155.80, 151.10, 146.89, 145.48, 135.08, 132.30, 130.21, 129.50, 124.36, 123.04, 120.11, 116.47, 114.62, 112.32, 66.97, 55.70, 50.09; HRMS (ES^+): m/z calculated for $C_{29}H_{26}F_3N_5O_4$: 588.1835 $[M+Na]^+$. Found 588.1832.

3,5-dimethoxy-N-(4-(4-methoxyphenoxy)-2-((4-morpholinophenyl)amino)pyrimidin-5-yl)benzamide (3h)

Yellowish white solid, yield 32.4%, mp: 208.7–210.0 °C. ^{1}H NMR (400 MHz, $CDCl_3$): δ 9.25 (s, 1H), 7.97 (s, 1H), 7.24 (d, 2H, *J* = 8.9 Hz), 7.12 (d, 2H, *J* = 9.0 Hz), 7.03 (d, 2H, *J* = 2.1 Hz), 7.00 (d, 2H, *J* = 9.0 Hz), 6.86 (s, 1H), 6.74 (d, 2H, *J* = 8.9 Hz), 6.63 (t, 1H, *J* = 2.1 Hz), 3.87–3.84 (m, 13H), 3.06 (t, 4H, *J* = 4.7 Hz); ^{13}C NMR (100 MHz, $CDCl_3$): δ 165.13, 161.09, 160.36, 157.38, 155.45, 150.55, 146.78, 145.55, 136.44, 132.48, 123.05, 119.98, 116.50, 114.57, 112.83, 105.14, 103.84, 66.97, 55.67, 50.14. HRMS (ES^+): m/z calculated for $C_{30}H_{31}N_5O_6$: 580.2172 $[M+Na]^+$. Found 580.2170.

3-methoxy-N-(4-(4-methoxyphenoxy)-2-((4-morpholinophenyl)amino)pyrimidin-5-yl)benzamide (3i)

White solid, yield 36%, mp: 185.0–185.5 °C. ^{1}H NMR (400 MHz, $CDCl_3$): δ 9.27 (s, 1H), 8.01 (s,1H), 7.49 (s, 1H), 7.45–7.38 (m, 2H), 7.24 (d, 2H, *J* = 9.0 Hz), 7.15–7.09 (m, 3H), 6.98 (d, 2H, *J* = 9.0 Hz), 6.85 (s, 1H), 6.74 (d, 2H, *J* = 8.9 Hz), 3.88–3.84 (m, 10H), 3.06 (t, 4H, *J* = 4.8 Hz); ^{13}C NMR (100 MHz, $CDCl_3$): δ 165.15, 160.36, 160.06, 157.40, 155.45, 150.57, 146.78, 145.57, 135.70, 132.49, 130.06, 129.85, 123.05, 119.99, 118.77, 118.20, 116.51, 114.59, 112.88, 112.64, 66.98, 55.70, 55.54, 50.15; HRMS (ES^+): m/z calculated for $C_{29}H_{29}N_5O_5$: 528.2247 $[M+H]^+$. Found 528.2244.

3,5-dimethoxy-N-(4-(4-methoxyphenoxy)-2-((6-(piperidin-1-yl)pyridin-3-yl)amino)pyrimidin-5-yl)benzamide (3j)

White solid, yield 64.3%, mp: 169.3–171.3 °C. ^{1}H NMR (400 MHz, $CDCl_3$): δ 9.21 (s, 1H), 8.02 (d, 1H, *J* = 2.3 Hz), 7.96 (s, 1H), 7.64 (dd, 1H, *J* = 9.0, 2.3 Hz), 7.09 (d, 2H, *J* = 9.0 Hz), 7.02 (d, 2H, *J* = 2.2 Hz), 6.96 (d, 2H, *J* = 9.0 Hz), 6.70 (s, 1H), 6.63 (t, 1H, *J* = 2.2 Hz), 6.48 (d, 1H, *J* = 9.1 Hz), 3.85 (s, 9H), 3.43–3.42 (m, 4H), 1.65–1.62 (m, 6H); ^{13}C NMR (100 MHz, $CDCl_3$): δ 165.15, 161.08, 160.48, 157.38, 156.46, 155.84, 150.64, 145.42, 139.56, 136.42, 130.50, 126.45, 122.93, 114.59, 112.96, 106.95, 105.14, 103.86, 55.67, 46.98, 25.50, 24.67; HRMS (ES^+): m/z calculated for $C_{30}H_{32}N_5O_5$: 557.2512 $[M+H]^+$. Found 557.2513.

N-(2-((4-fluorophenyl)amino)-4-(4-methoxyphenoxy)pyrimidin-5-yl)-3,5-dimethoxybenzamide (3k)

White solid, yield 72%, mp: 202.0–203.0 °C. ^{1}H NMR (400 MHz, $CDCl_3$): δ 9.29 (s, 1H), 7.99 (s, 1H), 7.26 (d, 2H, *J* = 9.0 Hz), 7.11 (d, 2H, *J* = 9.1 Hz), 7.03 (d, 2H, *J* = 2.2 Hz), 6.99 (d, 3H, *J* = 9.0 Hz), 6.84 (t, 2H, *J* = 8.6 Hz), 6.64 (t, 1H, *J* = 2.2 Hz), 3.88 (s, 3H), 3.86 (s, 6H); ^{13}C NMR (100 MHz, $CDCl_3$): δ 165.19, 161.13, 160.35, 159.33, 157.55, 156.94, 155.06, 150.39, 145.46, 136.34, 135.43, 123.05, 119.95, 119.87, 115.32, 115.10, 114.62, 113.35, 105.18, 103.90, 55.74, 55.69; HRMS (ES^+): m/z calculated for $C_{26}H_{23}FN_4O_5$: 491.1731 $[M+H]^+$. Found 491.1730.

3,5-dimethoxy-N-(4-(4-methoxyphenoxy)-2-((6-morpholinopyridin-3-yl)amino)pyrimidin-5-yl)benzamide (3l)

White solid, yield 55.9%, mp: 159.4–161.0 °C. ^{1}H NMR (400 MHz, $CDCl_3$): δ 7.99 (d, 1H, *J* = 2.6 Hz), 7.90 (s, 1H), 7.65 (dd, 1H, *J* = 9.0, 2.3 Hz), 7.03 (d, 2H, *J* = 9.0 Hz), 6.95 (d, 2H, *J* = 2.2 Hz), 6.90 (d, 2H, *J* = 9.0 Hz), 6.69 (s, 1H), 6.56 (t, 1H, *J* = 2.2 Hz), 6.40 (d, 1H, *J* = 9.0 Hz), 3.78 (s, 9H), 3.75 (t, 4H, *J* = 5.0 Hz), 3.33 (t, 4H, *J* = 5.0 Hz); ^{13}C NMR (100 MHz, $CDCl_3$): δ 165.15, 161.09, 160.45, 157.41, 155.95, 155.59, 150.51, 145.39, 139.31, 136.37, 130.16, 127.82, 122.93, 114.61, 113.20, 106.73, 105.15, 103.85, 66.78, 55.67, 46.28; HRMS (ES^+): m/z calculated for $C_{29}H_{30}N_6O_6$: 559.2305 $[M+H]^+$. Found 559.2301.

4.2. Biological evaluations

Detailed biological experimental data can be found in the supporting material.

Conflict of interest

The authors declare no conflict of interest.

Acknowledgment

This work was supported by the Creative Fusion Research Program through the Creative Allied Project funded by the National Research Council of Science & Technology (CAP-12-01-KIST) and by the KIST Institutional programs (Grant No. 2E28010) from Korea Institute of Science and Technology.

Abbreviations

AD, Alzheimer's disease; DAPK1, death-associated protein kinase 1; CSF1R, colony-stimulating factor-1 receptor; MAP, microtubule-associated protein; PSP, progressive supranuclear palsy; CBD, corticobasal degeneration; NFTs, neurofibrillary tangles; PDGFR, platelet-derived growth factor receptor; NO, nitric oxide; BiFC, bimolecular fluorescence complementation assay; RNS, reactive nitrogen species; LPS, lipopolysaccharides; DCM, dichloromethane; HRMS, high resolution mass spectrometry; NMR, nuclear magnetic resonance.

References

[1] K. Jin, J.W. Simpkins, X. Ji, M. Leis, I. Stambler, The Critical Need to Promote Research of Aging and Aging-related Diseases to Improve Health and Longevity of the Elderly Population, Aging and Disease, 6 (2015) 1-5.

[2] M.G. Spillantini, M. Goedert, Tau pathology and neurodegeneration, The Lancet. Neurology, 12 (2013) 609-622.

[3] T. Arendt, J.T. Stieler, M. Holzer, Tau and tauopathies, Brain research bulletin, 126 (2016) 238-292.

[4] D.R. Williams, Tauopathies: classification and clinical update on neurodegenerative diseases associated with microtubule-associated protein tau, Internal medicine journal, 36 (2006) 652-660.

[5] V.M. Lee, M. Goedert, J.Q. Trojanowski, Neurodegenerative tauopathies, Annual review of neuroscience, 24 (2001) 1121-1159.

[6] K. Iqbal, F. Liu, C.X. Gong, Tau and neurodegenerative disease: the story so far, Nature reviews. Neurology, 12 (2016) 15-27.

[7] N. Badiola, M. Suarez-Calvet, A. Lleo, Tau phosphorylation and aggregation as a therapeutic target in tauopathies, CNS & neurological disorders drug targets, 9 (2010) 727-740.

[8] A.K. Farag, E.J. Roh, Death-associated protein kinase (DAPK) family modulators: Current and future therapeutic outcomes, Med Res Rev, (2018);1–37. https://doi.org/10.1002/med.21518

[9] L.K. Chico, L.J. Van Eldik, D.M. Watterson, Targeting protein kinases in central nervous system disorders, Nature reviews. Drug discovery, 8 (2009) 892-909.

[10] A.M. Schumacher, A.V. Velentza, D.M. Watterson, Death-associated protein kinase as a potential therapeutic target, Expert Opin Ther Targets, 6 (2002) 497-506.

[11] B.M. Kim, M.H. You, C.H. Chen, S. Lee, Y. Hong, Y. Hong, A. Kimchi, X.Z. Zhou, T.H. Lee, Death-associated protein kinase 1 has a critical role in aberrant tau protein regulation and function, Cell death & disease, 5 (2014) e1237.

[12] L. Pei, S. Wang, H. Jin, L. Bi, N. Wei, H. Yan, X. Yang, C. Yao, M. Xu, S. Shu, Y. Guo, H. Yan, J. Wu, H. Li, P. Pang, T. Tian, Q. Tian, L.Q. Zhu, Y. Shang, Y. Lu, A Novel Mechanism of Spine Damages in Stroke via DAPK1 and Tau, Cerebral cortex (New York, N.Y. : 1991), 25 (2015) 4559-4571.

[13] S. Wang, X. Shi, H. Li, P. Pang, L. Pei, H. Shen, Y. Lu, DAPK1 Signaling Pathways in Stroke: from Mechanisms to Therapies, Molecular Neurobiology, 54 (2017) 4716-4722.

[14] H. Tsui, Q. Zeng, K. Chen, X. Zhang, Inhibiting Kinases in the CNS, in: S. Chackalamannil, D. Rotella, S.E. Ward (Eds.) Comprehensive Medicinal Chemistry III, Elsevier, Oxford, 2017, pp. 408-446.

[15] M.T. Heneka, M.J. Carson, J. El Khoury, G.E. Landreth, F. Brosseron, D.L. Feinstein, A.H. Jacobs, T. Wyss-Coray, J. Vitorica, R.M. Ransohoff, K. Herrup, S.A. Frautschy, B. Finsen, G.C. Brown, A. Verkhratsky, K. Yamanaka, J. Koistinaho, E. Latz, A. Halle, G.C. Petzold, T. Town, D. Morgan, M.L. Shinohara, V.H. Perry, C. Holmes, N.G. Bazan, D.J. Brooks, S. Hunot, B. Joseph, N. Deigendesch, O. Garaschuk, E. Boddeke, C.A. Dinarello, J.C. Breitner, G.M. Cole, D.T. Golenbock, M.P. Kummer, Neuroinflammation in Alzheimer's disease, The Lancet. Neurology, 14 (2015) 388-405.

[16] C. Laurent, L. Buee, D. Blum, Tau and neuroinflammation: What impact for Alzheimer's Disease and Tauopathies?, Biomedical Journal, 41 (2018) 21-33.

[17] I. Morales, L. Guzmán-Martínez, C. Cerda-Troncoso, G.A. Farías, R.B. Maccioni, Neuroinflammation in the pathogenesis of Alzheimer’s disease. A rational framework for the search of novel therapeutic approaches, Frontiers in Cellular Neuroscience, 8 (2014) 112.

[18] M.R. Bronzuoli, A. Iacomino, L. Steardo, C. Scuderi, Targeting neuroinflammation in Alzheimer’s disease, Journal of Inflammation Research, 9 (2016) 199-208.

[19] P. Parbo, R. Ismail, M. Sommerauer, M.G. Stokholm, A.K. Hansen, K.V. Hansen, A. Amidi, J.L. Schaldemose, H. Gottrup, H. Braendgaard, S.F. Eskildsen, P. Borghammer, R. Hinz, J. Aanerud, D.J. Brooks, Does inflammation precede tau aggregation in early Alzheimer's disease? A PET study, Neurobiology of disease, 117 (2018) 211-216.

[20] M.T. Heneka, M.K. O'Banion, D. Terwel, M.P. Kummer, Neuroinflammatory processes in Alzheimer's disease, J Neural Transm (Vienna), 117 (2010) 919-947.

[21] P. Johns, Chapter 8 - Cellular mechanisms of neurological disease, in: P. Johns (Ed.) Clinical Neuroscience, Churchill Livingstone, 2014, pp. 91-103.

[22] C.E.G. Leyns, D.M. Holtzman, Glial contributions to neurodegeneration in tauopathies, Molecular Neurodegeneration, 12 (2017) 50.

[23] J.D. Cherry, Y. Tripodis, V.E. Alvarez, B. Huber, P.T. Kiernan, D.H. Daneshvar, J. Mez, P.H. Montenigro, T.M. Solomon, M.L. Alosco, R.A. Stern, A.C. McKee, T.D. Stein, Microglial neuroinflammation contributes to tau accumulation in chronic traumatic encephalopathy, Acta Neuropathologica Communications, 4 (2016) 112.

[24] W.J. Streit, R.E. Mrak, W.S.T. Griffin, Microglia and neuroinflammation: a pathological perspective, Journal of Neuroinflammation, 1 (2004) 14.

[25] N. Maphis, G. Xu, O.N. Kokiko-Cochran, S. Jiang, A. Cardona, R.M. Ransohoff, B.T. Lamb, K. Bhaskar, Reactive microglia drive tau pathology and contribute to the spreading of pathological tau in the brain, Brain: a journal of neurology, 138 (2015) 1738-1755.

[26] W.-Y. Wang, M.-S. Tan, J.-T. Yu, L. Tan, Role of pro-inflammatory cytokines released from microglia in Alzheimer’s disease, Annals of Translational Medicine, 3 (2015) 136.

[27] S. Ghosh, M.D. Wu, S.S. Shaftel, S. Kyrkanides, F.M. LaFerla, J.A. Olschowka, M.K. O'Banion, Sustained interleukin-1beta overexpression exacerbates tau pathology despite reduced

amyloid burden in an Alzheimer's mouse model, The Journal of Neuroscience, 33 (2013) 5053-5064.

[28] R. von Bernhardi, J.E. Tichauer, J. Eugenin, Aging-dependent changes of microglial cells and their relevance for neurodegenerative disorders, Journal of Neurochemistry, 112 (2010) 1099-1114.

[29] Monica R.P. Elmore, Allison R. Najafi, Maya A. Koike, Nabil N. Dagher, Elizabeth E. Spangenberg, Rachel A. Rice, M. Kitazawa, B. Matusow, H. Nguyen, Brian L. West, Kim N. Green, Colony-Stimulating Factor 1 Receptor Signaling Is Necessary for Microglia Viability, Unmasking a Microglia Progenitor Cell in the Adult Brain, Neuron, 82 (2014) 380-397.

[30] D. Gomez-Nicola, N.L. Fransen, S. Suzzi, V.H. Perry, Regulation of microglial proliferation during chronic neurodegeneration, The Journal of Neuroscience, 33 (2013) 2481-2493.

[31] A. Martinez-Muriana, R. Mancuso, I. Francos-Quijorna, A. Olmos-Alonso, R. Osta, V.H. Perry, X. Navarro, D. Gomez-Nicola, R. Lopez-Vales, CSF1R blockade slows the progression of amyotrophic lateral sclerosis by reducing microgliosis and invasion of macrophages into peripheral nerves, Scientific Reports, 6 (2016) 25663.

[32] A. Olmos-Alonso, S.T.T. Schetters, S. Sri, K. Askew, R. Mancuso, M. Vargas-Caballero, C. Holscher, V.H. Perry, D. Gomez-Nicola, Pharmacological targeting of CSF1R inhibits microglial proliferation and prevents the progression of Alzheimer’s-like pathology, Brain: a journal of neurology, 139 (2016) 891-907.

[33] H. Asai, S. Ikezu, S. Tsunoda, M. Medalla, J. Luebke, T. Haydar, B. Wolozin, O. Butovsky, S. Kügler, T. Ikezu, Depletion of microglia and inhibition of exosome synthesis halt tau propagation, Nature Neuroscience, 18 (2015) 1584-1593.

[34] A. Anighoro, J. Bajorath, G. Rastelli, Polypharmacology: challenges and opportunities in drug discovery, Journal of Medicinal Chemistry, 57 (2014) 7874-7887.

[35] M.L. Bolognesi, Polypharmacology in a single drug: multitarget drugs, Current Medicinal Chemistry, 20 (2013) 1639-1645.

[36] T.S. Wilbek, T. Skovgaard, F.J. Sorrell, S. Knapp, J. Berthelsen, K. Stromgaard, Identification and characterization of a small-molecule inhibitor of death-associated protein kinase 1, Chembiochem: a European journal of chemical biology, 16 (2015) 59-63.

[37] A.K. Farag, A. Elkamhawy, A.M. Londhe, K.-T. Lee, A.N. Pae, E.J. Roh, Novel LCK/FMS inhibitors based on phenoxypyrimidine scaffold as potential treatment for inflammatory disorders, European Journal of Medicinal Chemistry, 141 (2017) 657-675.

[38] T.M. Ballard, G.A. Higgins, T. Hoffmann, S.M. Poli, A. Sleight, Preparation of 2-[3,5-bis(trifluoromethyl)phenyl]-N-methyl-N-[6-(morpholin-4-yl)-4-(o-tolyl)-pyridin-3-yl]-isobutyramide for the treatment of diseases related to the NK-1 receptor, in, F. Hoffmann-La Roche A.-G., Switz. . 2001, pp. 12 pp.

[39] D. Bhattarai, J.H. Jung, S. Han, H. Lee, S.J. Oh, H.W. Ko, K. Lee, Design, synthesis, and biological evaluation of structurally modified isoindolinone and quinazolinone derivatives as hedgehog pathway inhibitors, European Journal of Medicinal Chemistry, 125 (2017) 1036-1050.

[40] C.-Y. Sun, Y.-S. Li, A.-L. Shi, Y.-F. Li, R.-F. Cao, H.-W. Ding, Q.-Q. Yin, L.-J. Zhang, H.-C. Zheng, H.-R. Song, Synthesis and antiproliferative activity of novel 4-substituted-phenoxy-benzamide derivatives, Chin. Chem. Lett., 26 (2015) 1307-1310.

[41] H. Ma, S. Deacon, K. Horiuchi, The challenge of selecting protein kinase assays for lead discovery optimization, Expert Opinion on Drug Discovery, 3 (2008) 607-621.

[42] S. Lim, M.M. Haque, D. Kim, D.J. Kim, Y.K. Kim, Cell-based Models To Investigate Tau Aggregation, Comput. Struct. Biotechnol. J., 12 (2014) 7-13.

[43] H. Tak, M.M. Haque, M.J. Kim, J.H. Lee, J.-H. Baik, Y. Kim, D.J. Kim, R. Grailhe, Y.K. Kim, Bimolecular Fluorescence Complementation; Lighting-Up Tau-Tau Interaction in Living Cells, PLOS ONE, 8 (2013) e81682.

[44] Y.J. Zhang, Y.F. Xu, Y.H. Liu, J. Yin, J.Z. Wang, Nitric oxide induces tau hyperphosphorylation via glycogen synthase kinase-3beta activation, FEBS letters, 579 (2005) 6230-6236.

[45] M. Takahashi, Y. Chin, T. Nonaka, M. Hasegawa, N. Watanabe, T. Arai, Prolonged nitric oxide treatment induces tau aggregation in SH-SY5Y cells, Neuroscience Letters, 510 (2012) 48-52.

[46] J.E. Yuste, E. Tarragon, C.M. Campuzano, F. Ros-Bernal, Implications of glial nitric oxide in neurodegenerative diseases, Frontiers in Cellular Neuroscience, 9 (2015) 322.

[47] K.M.K. Boje, Neurotoxic Mechanisms of Nitric Oxide, in: P.L. Wood (Ed.) Neuroinflammation: Mechanisms and Management, Humana Press, Totowa, NJ, 2003, pp. 117-135.

[48] T. Horiguchi, K. Uryu, B.I. Giasson, H. Ischiropoulos, R. LightFoot, C. Bellmann, C. Richter-Landsberg, V.M. Lee, J.Q. Trojanowski, Nitration of tau protein is linked to neurodegeneration in tauopathies, The American Journal of Pathology, 163 (2003) 1021-1031.

[49] M.R. Reynolds, J.F. Reyes, Y. Fu, E.H. Bigio, A.L. Guillozet-Bongaarts, R.W. Berry, L.I. Binder, Tau nitration occurs at tyrosine 29 in the fibrillar lesions of Alzheimer's disease and other tauopathies, The Journal of Neuroscience, 26 (2006) 10636-10645.

[50] R.P. Patel, J. McAndrew, H. Sellak, C.R. White, H. Jo, B.A. Freeman, V.M. Darley-Usmar, Biological aspects of reactive nitrogen species, Biochimica et Biophysica Acta, 1411 (1999) 385-400.

[51] K.M. Boje, Nitric oxide neurotoxicity in neurodegenerative diseases, Frontiers in Bioscience: a journal and virtual library, 9 (2004) 763-776.

[52] K. Ackerman, J. Fiddler, T. Soh, S. Clarke, BV-2 Microglial Cells Used in a Model of Neuroinflammation, The FASEB Journal, 29 (2015) 608.602.

[53] T. Danker, C. Möller, Early identification of hERG liability in drug discovery programs by automated patch clamp, Frontiers in Pharmacology, 5 (2014) 203.

[54] B. London, M.C. Trudeau, K.P. Newton, A.K. Beyer, N.G. Copeland, D.J. Gilbert, N.A. Jenkins, C.A. Satler, G.A. Robertson, Two isoforms of the mouse ether-a-go-go-related gene coassemble to form channels with properties similar to the rapidly activating component of the cardiac delayed rectifier K+ current, Circ Res, 81 (1997) 870-878.

[55] M.C. Sanguinetti, M. Tristani-Firouzi, hERG potassium channels and cardiac arrhythmia, Nature, 440 (2006) 463.

[56] B. Priest, I.M. Bell, M. Garcia, Role of hERG potassium channel assays in drug development, Channels, 2 (2008) 87-93.

[57] V.B. Siramshetty, J. Nickel, C. Omieczynski, B.-O. Gohlke, M.N. Drwal, R. Preissner, WITHDRAWN—a resource for withdrawn and discontinued drugs, Nucleic acids research, 44 (2016) D1080-D1086.

[58] M. Kansy, F. Senner, K. Gubernator, Physicochemical High Throughput Screening: Parallel Artificial Membrane Permeation Assay in the Description of Passive Absorption Processes, Journal of Medicinal Chemistry, 41 (1998) 1007-1010.

[59] A. Grosdidier, V. Zoete, O. Michielin, SwissDock, a protein-small molecule docking web service based on EADock DSS, Nucleic Acids Res, 39 (2011) W270-277.

[60] A. Grosdidier, V. Zoete, O. Michielin, Fast docking using the CHARMM force field with EADock DSS, J Comput Chem, 32 (2011) 2149-2159.

[61] I. de Diego, J. Kuper, N. Bakalova, P. Kursula, M. Wilmanns, Molecular Basis of the Death-Associated Protein Kinase–Calcium/Calmodulin Regulator Complex, Sci. Signal., 3 (2010) ra6-ra6.

[62] A. Elkamhawy, A.K. Farag, A.N.I. Viswanath, T.M. Bedair, D.G. Leem, K.-T. Lee, A.N. Pae, E.J. Roh, Targeting EGFR/HER2 tyrosine kinases with a new potent series of 6-substituted 4-anilinoquinazoline hybrids: Design, synthesis, kinase assay, cell-based assay, and molecular docking, Bioorganic & Medicinal Chemistry Letters, 25 (2015) 5147-5154.

List of Captions

Figure 1. The proposed design of DAPK1-CSF1R dual inhibitors.

Figure 2. Dose-response curves for the impact of compound **3l** on the kinase reaction of DAPK1 at 1, 10, and 100 μM concentrations of ATP.

Figure 3. Dose-response curves for the impact of **3l** on the CSF1R kinase reaction at 1, 10, and 100 μM concentrations of ATP.

Figure 4. Effects of DAPK1 inhibitors on tau aggregation. HEK293 tau-BiFC cells were treated with each compound in various concentrations in the presence of forskolin (30 μM) for

48 h. Data are mean ± SD. The intensity of BiFC fluorescence was quantified by using a Harmony 3.1 software (PerkinElmer^{TM}).

Figure 5. Effects of compounds **3h** and **3l** on LPS-induced BV-2 cell line. A) Inhibition of NO production in LPS-stimulated BV-2 cell line by compounds **3h** and **3l**. Values are the means of five independent experiments ± SD. B) the impact of for compounds **3h** and **3l** on the viability of BV-2 cell line. Values are the means of five independent experiments ± SD.

Figure 6. Selectivity profile elicited by 10 μM concentration of compound **3l** against a panel of 47 kinases including CSF1R and DAPK1. These data are the mean of two independent experiments ± standard deviation.

Figure 7. The ATP-binding site and the substrate-binding sites of the DAPK1 protein. A hydrophobic surface was generated around the protein using Discovery studio program standard protocol for surface generation.

Figure 8. *In silico* calculated binding modes of compound **3l** within DAPK1. A) Calculated binding mode of **3l** within the substrate-binding site of DAPK1. B) Calculated binding mode of **3l** within the ATP-binding site of DAPK1.

Figure 9. *In silico* calculated binding modes of compound **3g** within DAPK1. A) Calculated binding mode of **3g** within the substrate-binding site of DAPK1. B) Calculated binding mode of **3g** within the ATP-binding site of DAPK1.

Figure 10. *In silico* calculated binding modes of compound **3l** within the ATP pocket of the CSF1R kinase (pose No. 3) showing regular binding mode with the 3,5-dimethoxyphenyl moiety embedded deep inside the hydrophobic pocket of the ATP binding site.

Table 1. Substitution pattern, Percent inhibition values and IC_{50} values for the newly synthesized compounds over CSF1R and DAPK1.

Table 2. hERG channel affinity data (as IC_{50} value) of compound **3l**.

Scheme 1. Synthesis of compounds **3a–l**.

Scheme 2. Synthesis of compounds **9a–c**.

- Multifunctional DAPK1 and CSF1R inhibitors for targeting tauopathies.
- **3l** shows good potency and excellent affinity and within-family selectivity for both kinases.
- Mechanistic study showed **3l** as non-ATP-competitive DAPK1 inhibitor and ATP-competitive CSF1R inhibitor.
- **3l** has tau aggregation inhibition and anti-neuroinflammatory activity in cellular assays.
- hERG binding and PAMPA assays revealed **3l** as a cardiosafe and has a high membrane penetration.